Methodological approaches to study antibody aggregation and thermal stability

Master's thesis

Suvituuli Poikonen

[1]Detection Technology

Department of Chemistry

University of Turku

[2]Orion Corporation

Tengströminkatu 8

20360 Turku

May 2022

Master's thesis

Subject: Chemistry
Author: Suvituuli Poikonen[1]
Title: Methodological approaches to study antibody aggregation and thermal stability
Supervisors: Harri Härmä[1], Kari Kopra[1], Mikko Ares[2], and Rune Salbo[2]
Number of pages: 52
Date: May 2022

Therapeutic monoclonal antibodies are alluring novel drug candidates for the treatment of various diseases, but their complicated structures also present challenges in meeting the stability requirements of drugs. The utility of external luminescent probes in the detection of protein aggregates compared to common methods of SEC-MALS and DLS used in the pharmaceutical industry was assessed in this study. The methods were compared in terms of sensitivity, specificity towards different aggregates, and overall performance. Also, the applicability of different (nano)DSF methods was compared in producing thermal unfolding curves of the chosen antibodies.

Luminescent probes proved their applicability and high sensitivity in aggregation studies while problems with the more established light scattering-based methods surfaced. The probes were able to produce quantitative results for the samples, while SEC-MALS detected aggregation primarily as reduced content of the intact protein. DLS produced qualitative results but suffered from low resolution. Multiple analytical methods are still required to confirm the results from aggregate studies due to the dynamic and complicated nature of aggregates. In the thermal unfolding experiments, nanoDSF reliably produced unfolding curves for all the studied mAbs without external components. The external probes had more variance between different mAbs, which was reflected in the unfolding curves. However, the lowest LLD was achieved with a FRET-probe that utilizes the long lifetime of Eu^{3+}-chelate emission.

Keywords: aggregation, antibody, DLS, external probes, light scattering, luminescence, MALS, size-exclusion chromatography, thermal unfolding

Table of contents

Abbreviations

(T)ICT = (Twisted) Intramolecular Charge Transfer

ANS = 8-Anilino-1-naphthalenesulfonate

AT = Aggregated Trastuzumab

CDR = Complementary Determining Region

CV % = Coefficient of Variation %

DLS = Dynamic Light Scattering

dRI = differential Refractive Index

DSF = Differential Scanning Fluorimetry

D_T = Translational diffusion coefficient

EMA = European Medicines Agency

ET = Energy Transfer

Fab = Fragment antigen binding

Fc = Fragment crystallizable

FDA = U.S. Federal Drug and Food Administration

GMP = Good Manufacturing Practices

HMWA = High Molecular Weight Aggregates

Ig = Immunoglobulin

ISC = Intersystem crossing

IV = Viscometer

LLD = Lower Limit of detection

mAb = Monoclonal antibody

MALS = Multi-Angle Light Scattering

MS = Mass spectrometer

MW = Molecular Weight

MWCO = Molecular weight cutoff

PDI = Polydispersity Index

PS = ProteoStat

QC = Quality control

RET = Resonance Energy Transfer

Rg = Radius of gyration

rH = Hydrodynamic radius

RI = Refractive Index

rpm = rounds per minute

S/B = Signal-to-Background

SD = Standard Deviation

SEC = Size-Exclusion Chromatography

T_m = Midpoint melting temperature

T_{onset} = Onset melting temperature

TR-FRET = Time-Resolved Förster Resonance Energy Transfer

TRL = Time-resolved Luminescence

UV = Ultraviolet

1 Introduction

1.1 Antibody aggregation

Therapeutic monoclonal antibodies (mAbs) are immunoglobulins (Ig) consisting of a protein structure with attached carbohydrates. The most common immunoglobulin isotype utilized in therapeutic applications is IgG, that is built of four polypeptide chains, two heavy chains and two light chains. The heavy chains consist of four domains and the light chains of two. The structure can be divided into two fragment antigen binding (Fab) -portions and one fragment crystallizable (Fc) -portion. Disulfide bonds connect the light and heavy chains in the Fab-portions and the two heavy chains in the Fc-portion, near a hinge region that connects the Fabs to the Fc. The variable regions at the ends of the Fabs contain complementary determining regions (CDRs), which are responsible for the antigen binding of the molecule, while Fc-portion mediates effector functions. The structure of a mAb molecule is presented in *Figure 1*. Common carbohydrates in humans attached to the IgGs are e.g., galactose, fucose, mannose and N-acetylglucosamine.
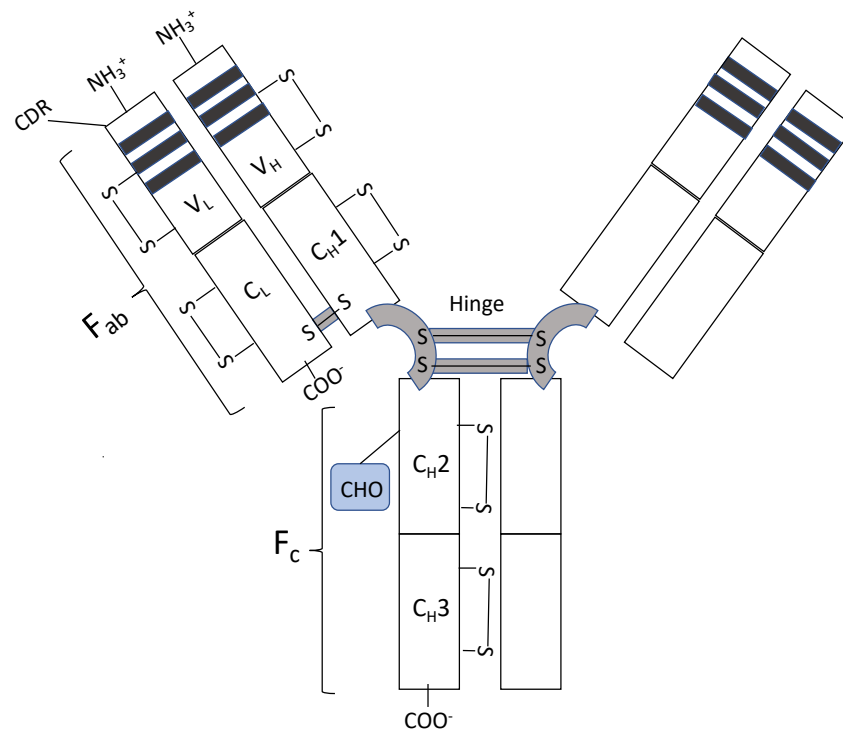
Figure 1. Structure of an IgG antibody. (Abbreviations: CH: constant domain, heavy chain, CL: constant domain, light chain, VH: variable domain, heavy chain, VL: variable domain, light chain, Fc: fragment crystallizable, Fab: fragment antigen-binding, COO-: carboxy terminal, NH3+ amino terminal, CDR: complementary determining region, S-S: disulfide bond). IgGs have a molecular weight of approximately 150 kDa and dimensions in the nanometer scale. The figure is adapted from Awwad, S., *et al.*, *Pharm*. **2018**, *10*, 83.

Therapeutic mAbs are currently used to treat a vast variety of diseases ranging from autoimmune diseases and inflammations to different cancers. They can mediate their therapeutic effect by e.g., causing cell death of the bound target. Currently over 100 therapeutic antibody drugs have been either approved or are under review by European Medicines Agency (EMA) or by the U.S. Federal Drug and Food Administration (FDA)[1], with estimates of rapid market growth[2]. Mabs are attractive drug candidates since they possess high specificity and affinity towards their drug targets, with affinities varying typically between pico- to nanomolar[3]. Also, due to similarities in the constant domains of mAbs and the use of platform-based manufacturing processes, they are alluring biological drug options against new targets. As protein-based therapeutics, their structure is complex and large, which possesses challenges throughout the drug development process. Sample heterogeneity is problematic, stemming from different phases of the drug manufacturing process or variations in the formulation. Different techniques and quality control steps in the manufacturing processes are utilized to minimize heterogeneity in addition to optimal drug formulations that ensure the integrity of the drug even when submitted to different stress conditions. Not only does sample heterogeneity impose safety issues and increased immunogenicity, but it also affects the efficacy and activity of the drug. Regulatory agencies like EMA and FDA have implemented Good Manufacturing Practices (GMP), which manufacturers must comply with and get approved for. These strict guidelines ensure product safety and quality, among other factors, and emphasize the importance of sample homogeneity.[2]

Different physical stress factors occur at multiple phases of the mAb manufacturing process, resulting in non-native mAb structures. The most common stresses that mAbs encounter throughout their life cycle are mechanical stress, temperature changes, and freeze–thaw cycles[4]. Another major factor causing drug instability and variation is formulation. Formulation is a process where different chemical substances are combined with the active pharmaceutical ingredient to obtain a final product. Solubility, viscosity, and aggregation are the main concerns in formulation development[2], and it is highly dependent on the route of administration of the drug. Sample homogeneity can be achieved by creating a stable product that is not prone to degradation and/or aggregation. The protein instability mechanisms can be divided into physical and chemical instabilities, which may be sometimes hard to separate since one can lead to the other. Examples of chemical degradations of mAb therapeutics are oxidation, deamidation and, cross-linking. Physical degradation stems from the loss of the three-dimensional

structure, induced by different environmental factors or by previously mentioned chemical instabilities. One significant physical degradation is the formation of aggregates.[5]

The native mAb structures are held together by various non-covalent forces, including van der Waals, electrostatic and hydrophobic interactions, and hydrogen bonds. Within a native, folded mAb, some forces resist the folding, including steric and electrostatic repulsions and the loss of entropy. The tertiary structure of a mAb is in a dynamic equilibrium and fluctuations between the folded and slightly unfolded states occur.[6] Even slight changes to this equilibrium can cause the structure of a mAb to change towards a more unstable form. This makes the structure of mAbs, and proteins in general, inherently quite unstable.[7] Protein stability can be divided into conformational and colloidal stability. Conformational stability relates to the forces keeping a protein in its folded form, and colloidal stability relates to the interactions between individual proteins[8]. An intermediate state, like a molten globule, can lead to an unstable structure. These unstable structures can achieve lower free energy by assembling and forming aggregates. Native monomers may also assemble to aggregates, and so it is a term describing a complex of at least two monomers. The forces holding these monomers together can be covalent or non-covalent, and some aggregates can be reversibly self-associated.[3] Reversibility of aggregates is dependent on, e.g., the sample matrix and this feature may change upon alteration of conditions. The lifetimes of reversible aggregates vary significantly from milliseconds to days.[9]

Nucleation is described as the preliminary event in the formation of aggregates. It can originate from an exposure of an aggregation-prone sequence often called 'hot spot' due to natural conformational fluctuations of mAbs. Exposure of these sequences can cause the association of monomers to form oligomers and eventually reversibly dissociate back to monomers. Once first irreversible aggregates form, e.g., via beeta-sheet formation with other monomers, they are called nuclei.[6] Different stress factors, like inappropriate formulation[10] or physical stress[11], can enhance disruptions in the mAb structures and increase the nucleation events. In addition to disintegration in the structures, intermolecular bonds, e.g., disulfide bonds, can form via reactions between native mAbs, which can also induce aggregation[12]. Hydrophobic interactions have been traditionally proposed as the driving forces for aggregation. In addition, electrostatic interactions can also be named an essential force in aggregates' formation.[13] The driving force(s) in protein aggregation are dependent, e.g., on the environment and the protein structure, and are

case-dependent[8]. In general, the aggregation process is a sum of various factors. The rate might be impossible to estimate based only on the structure of the studied protein[14] since environmental factors play a crucial role. For protein-based drugs, aggregation propensity is a combination of nucleation, conformation, and colloidal effects[15]. Aggregation can be concentration-dependent or -independent. Especially with mAbs, it has been observed that high concentrations can increase the rate of aggregation or promote it due to shorter distances between the molecules.[8] Concentration independent aggregation is observed when the aggregation is due to unfolding processes[16] or adsorption to bulk surfaces[17].

The formed oligomers can grow into larger particles via various mechanisms, e.g., aggregate-aggregate interactions[18], condensation[18], chain-polymerization[19], or monomer addition[19]. The growth of aggregates is usually not a linear process in relevance to time. The growth can even be exponential as the number of aggregates grows. These additional aggregates and nuclei can be described as seeds that ease the growth of aggregates. The aggregates become first become subvisible, and thereafter possibly visible as they are no longer soluble. Eventually, they may sediment.[8] An example of aggregation pathways is presented in *Figure 2*.

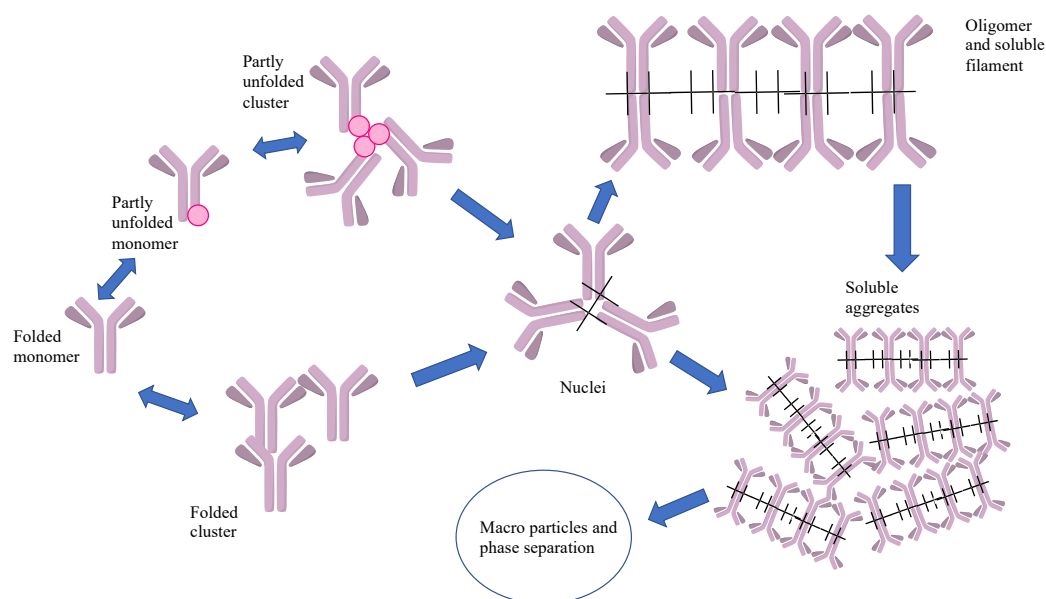*Figure 2*. A schematic representation of possible aggregation pathways of an antibody. The pink circles symbolize 'hot spot' sequences that are usually buried in the structures but upon exposure can form intermolecular bonds. The single arrows represent irreversible steps and double arrows reversible steps. The figure is adapted from Roberts, C. J., *Trends Biotechnol.,* **2014**, *32*, 372–380.

General classes of aggregates have been specified as follows[9]: 1) swiftly reversible noncovalent small oligomers (dimers, trimers, etc.); 2) irreversible noncovalent oligomers; 3) covalent oligomers; 4) large aggregates (over 10-mer); 5) very large aggregates (from 50 nm to 3 μm); 6) visible particulates. The reversibility of the larger aggregates depends on the type of interaction(s) involved in the structure. A sample containing aggregates is likely to include more than one type of the following aggregates.[9]

Multiple analytical methods are usually required to make a definite conclusion on the stability of the product. For aggregation studies, at least Size-Exclusion Chromatography (SEC) and turbidity measurements are recommended, but additional complementary methods are also advised to support the decision making.[20] It is noteworthy that different analytical techniques can give different results based on their operation time due to the varying lifetimes of reversible aggregates. It is also essential that the method does not induce or destroy aggregates for accurate aggregate detection.[9] An analytical method would ideally give the exact amount by weight fraction and size of all the species present in a sample. However, more commonly, the methods report the total amount of aggregates and main size classes in relation to the native mAb.[21]

1.2 The purpose and goal of the work

The purpose of this master's thesis was to study and compare different analytical methods in the detection of monoclonal antibody aggregates and test different (nano) Differential Scanning Fluorimetry (DSF) methods in the production of thermal unfolding curves of the studied mAbs. The studied monoclonal antibodies were trastuzumab (hIgG1), atezolizumab (mIgG2a), pembrolizumab (hIgG1), bococizumab (hIgG1) and antibody X (mIgG1). The work comprised of two main parts. First, thermal unfolding curves of the mAbs using (nano)DSF methods were measured. This was performed to observe differences in the melting curves when measured using different external luminescent probes or the inherent luminescence of the antibodies. In addition to their overall performance, the methods were evaluated in terms of their sensitivity and selectivity. The melting curves were obtained using nanoDSF with Prometheus Panta -instrumentation and with ANS, SYPRO Orange, and FRET-probe that bind to antibodies upon structural changes. In this experiment, the five antibodies studied were chosen based on distinguishable melting curves and concentration dependency observation with the obtained T_m-values using nanoDSF. A T_m-value indicates the temperature at which half of the mAb molecules have unfolded.

The second part of the work comprised physically induced aggregation of the studied mAbs and subsequent analysis of the mAbs carried out with selected methods. The biophysical techniques used in this study were SEC combined with Multi-Angle Light Scattering (MALS), Dynamic Light Scattering (DLS), and external luminescent probes ProteoStat, Protein-Probe, and SYPRO Orange. The DLS studies were run in a batch mode with a dedicated instrument, while SEC-MALS, also having a DLS module, was used in a flow mode. However, in this study, emphasis was placed on the batch mode DLS. The aim was to compare the selected methods in their ability to detect antibody aggregation and measure different forms of aggregates. Emphasis was also placed on the sensitivities of the methods. The amount of aggregates were evaluated with the help of aggregation-% standards, commercial and self-produced. With common analytical methods used in the pharmaceutical industry, like SEC-MALS and DLS, external probes as complementary methods in analyzing mAb aggregates were assessed. An additional goal of the study was to obtain more information on the mAb aggregation processes, which was performed by a slow induction of aggregates with two mAb samples and by monitoring the events over days. Also, the relationship between conformational stability obtained with (nano)DSF-methods and the aggregation tendency of the mAbs was examined, although only a modest correlation has been previously discovered[22].

1.3 Methods for thermal unfolding

Thermal unfolding is a process where proteins lose their native three-dimensional structure upon exposure to gradually rising temperatures. This change from their folded structure to a fully unfolded state can be monitored with multiple methods. One popular method is DSF, which utilizes external luminescent probes to visualize the thermal unfolding process. These probes bind to the exposed parts of proteins as they unfold. The prefix nano- is used when the luminescence is produced by the intrinsic fluorophores in the protein structure, and no external probes are utilized. Common parameters derived from the unfolding process are the onset (T_{onset}) and midpoint (T_m) temperatures of the specific protein, indicating the temperatures at which the unfolding has begun and at which half of the studied protein molecules have unfolded. A high T_m-value represents high conformational stability. This information can partly be used to explain aggregation.

In DSF, multiple different types of external probes can be utilized. Depending on the probe, it can function, e.g., by hydrophobic interactions or by detecting changes in the solvent viscosity. The luminescence emission and the wavelength maximum of the probe

change as the protein unfolds. In nanoDSF, the 350/330 nm is measured, and changes in the ratio can be seen when the polarity of the microenvironment around the aromatic amino acids, mostly tryptophan, alter[23]. Usually, the F350/330 nm increases when a protein unfolds since a red shift occurs when tryptophan is exposed to a more polar environment[24]. The F350/330 nm is a global average of all the local surroundings in the studied molecule. Multiple events can affect the luminescence intensity and wavelength maxima, like aggregation and different quenching effects, and these complicated spectroscopic events hamper the data interpretation. Also, sometimes tryptophan residues might move towards a more hydrophobic environment in an unfolding event, which can be seen as a blue shift.[23]

The luminescence sensitivity enables the detection of unfolding events of individual domains, which is highly beneficial with multidomain proteins like mAbs. Three unfolding events may be seen with mAbs. These represent three different mAb regions/domains, which usually unfold in the following order: CH2, Fab, and CH3[25]. However, not all of these events are always measurable since e.g. the subclass of IgG or the stability of the Fab region affects the measurement[23]. Additional orthogonal methods, like DLS, can provide insightful information about the aggregation propensity of different domains and help pinpoint where possible engineering efforts should be directed.

1.4 Methods for aggregation

1.4.1 Size-exclusion chromatography and light scattering-based methods

Size-exclusion chromatography is used as a standard method to assess aggregate levels qualitatively and quantitatively in protein therapeutics. It separates proteins based on their molecular sizes (hydrodynamic radius, r_H) and diffusivities and is an entropically driven separation method where no adsorption should occur. The stationary phase consists of densely packed small, porous particles through which the proteins diffuse. The pore size is selected according to the sample, and the elution order follows the order of decreasing size. Proteins larger than the pores are excluded and elute out first with the interstitial volume. The mobile phase is usually a buffered aqueous solution with a neutral pH. One of the advantages of SEC is the close physiological conditions that can be achieved with the mobile phase. With these conditions, any conformational changes upon mAb structures are mitigated, which could significantly impact the separation process.[26] In terms of aggregate characterization, SEC is commonly used to separate different sample species due to its sensitivity, simplicity, moderate throughput, and applicability to a QC

environment.[21] SEC is also compatible with various combinations of detectors like UV, MALS, viscometer (IV) and differential refractive index (dRI), which allow a comprehensive evaluation of the mAb samples[27]. Additional information about the hydrodynamic sizes of the aggregates can be obtained by connecting DLS to the system[28], and a complete structural characterization is also achievable by combining SEC with a mass spectrometer (MS)[26].

SEC-MALS is a general name for a configuration comprising of SEC used with MALS, dRI, and UV detectors. The aromatic amino acids in the mAb structure absorb UV light at around 280 nm[29], and it is a standard detector coupled with SEC to visualize the peaks and determine concentrations. dRI detector is also used to determine sample concentrations, as it detects changes in the refractive index of the eluent due to samples eluting. Multi-angle light scattering detector allows to obtain the molecular weights (MW) and the mean square radius of the eluting components with the help of the information from the other detectors. It measures the amount of light scattered into different angles when an analyte is irradiated with a laser beam.[30] The number of photodiodes can vary from 3 to around 20.[31] The MWs of the eluting components can be calculated based on Equation (1),

$$M = \frac{R(0)}{Kc(\frac{dn}{dc})^2} \quad (1)$$

where M is the molecular weight of the analyte, $R(0)$ is the reduced Rayleigh ratio (amount of scattered light relative to the laser intensity) extrapolated to zero angle, c is the concentration based on either the UV or dRI detector, dn/dc is the increase in the refractive index and K is a system constant[32]. The concentration is usually calculated based on the dRI[30], since the concentration-response dn/dc is similar for almost all pure proteins in aqueous buffer[33]. An SEC-MALS configuration allows the determination of MWs without regarding the elution volumes. This eliminates possibly wrong derived MWs if the calculations were performed using a standard curve based on a globular reference protein and can be considered an 'absolute' method.[30] With an additional DLS detector, information can also be obtained about the conformation and hydrodynamic sizes of the particles[28].

In light scattering applications, a liquid sample is irradiated with a monochromatic laser, and the light is scattered in all directions due to the solvent and particles. The shape and the size of the analyzed molecules affect how the light scatters. This scattered light is detected by photodetectors placed around the sample. The information generated from

this application is based on the Brownian motion of particles in solution, which results from coincidental collisions between the particles and solvent molecules. The Brownian motion will cause the scattered light intensity to fluctuate in relation to time, and the particle size will affect the time of these intensity fluctuations. In multi-angle light scattering, a time-averaged intensity is recorded at different angles θ related to the sample. The smaller the angle of scattered light, the higher the intensity and vice versa.[28] The asymmetry grows in proportion to the particle size. With this information, the weight-averaged molar mass and mean square radius, also known as the radius of gyration (R_g), can be determined with the knowledge of concentration from MALS[32].

With DLS, the occurring intensity fluctuations are characterized. The smaller the particles are, the faster intensity fluctuations occur and vice versa. These fluctuations are recorded to time, and with the help of autocorrelation analysis, translational diffusion coefficients (D_T) for the particles can be derived. This way, size distributions and hydrodynamic particle sizes for samples can be obtained.[28] DLS covers particle size range between 0.3 nm – 10 μm[34]. With the translational diffusion coefficient, the hydrodynamic radius of the particle can be determined, which is defined as a hard-sphere with the same diffusion coefficient as the particle in question.[28] The r_H can be derived from the Stokes-Einstein Equation[35] (2),

$$D_T = \frac{k_B T}{6\pi\eta R_h} \quad (2)$$

where k_B is Boltzmann coefficient, T is temperature (K) and η is the viscosity of the medium.

Both MALS and DLS are non-invasive, which is essential when reliable results from sensitive samples, like aggregates, are desired.[15,36] Both methods are also inherently biased towards higher molecular weight species. The higher the molecular weight of the component, the higher the scattering intensity. This means that when, e.g., the size distribution of a sample is analyzed with DLS, the high molecular weight aggregates (HMWA, > 100 nm) are disproportionally represented over the possibly dominant, smaller molecular weight components. Also, the concentration of the molecules affects the signal intensity. This way, these light scattering methods can detect even a small amount of aggregates in a sample, but they are also sensitive to contaminants, other interfering particles, and air bubbles.[36]

DLS is considered exceptionally useful in detecting subvisible particles in protein therapeutics, which often can act as nuclei for visible particles. DLS is ideal for these samples since the subvisible precursors are usually present at very low levels initially but might accumulate in storage and cause the formation of visible particulates with time. Due to this, DLS is best suited for studying larger aggregates.[9] When DLS is combined with SEC, it is used in flow mode, but the method is often used in batch mode. The advantages of batch mode detection are the lack of separation and dilution, which means that the reversible aggregates are in equilibrium.[21] Also, the sample consumption in batch mode is small, and it is applicable for a high-throughput method[36]. In general, the large dynamic size and concentration range of DLS[21] are clear benefits of the method.

Limitations of DLS are that it suffers from low resolution meaning that it has trouble separating molecules of similar size, like a monomer from a dimer[36]. Reports of a minimum size difference that DLS can resolve vary from fivefold[37] to tenfold[34]. It is also sensitive to solvent viscosity and temperature, which must be known for reliable measurements[36]. In addition, turbid[36] and concentrated[15] samples cause problems in the experiments. With concentrated samples, particle-particle and particle-solvent interactions might cause deviation in the obtained particle sizes[21]. It has been reported that the method underestimates the particle size at high concentrations and overestimates it at low concentrations.[34] An instrument-specific concentration working range for different particle sizes needs to be established to determine the correct particle sizes. The DLS used in batch mode also suffers from masking due to the bias towards large particles. Especially with highly aggregated samples, smaller aggregates might be masked. DLS has been reported to not be optimal for analyzing polydisperse samples due to the low resolution and concentration dependency. This suggests that inaccurate results are possible when analyzing aggregated mAb samples with DLS.[34] It is also noteworthy that while DLS can be considered a high-throughput method, the throughput is affected by laborious data interpretation.[21]

Most of the drawbacks of SEC-MALS in characterizing protein aggregates are rooted in SEC alone. SEC has a limited dynamic range, which negatively correlates with the resolution of the system.[21] Unwanted interactions between the stationary phase and mAbs may occur and cause asymmetry in the peaks, lower recovery, and altered elution times[26]. The main interactions in question are hydrophobic and electrostatic interactions[38]. The attempts to mitigate these secondary interactions can involve changes in the mobile phase[26] by, e.g., an increase in the ionic strength, which might affect the sample

composition by inducing additional aggregate formation[9]. Also, the usage of high-pressure columns can falsify the test results by creating new aggregates. A study showed that SEC columns with particle sizes below 2 μm increased pressure and subsequently the aggregate amount.[39] Also, changes in the solubility of mAbs are relevant when high pressures are used[26]. SEC also suffers from moderate throughput due to the high resolution required from the method[26]. In addition, the samples are filtered and highly diluted in the separation process, which could cause the dissociation of reversible aggregates[38]. The inherent lifetimes of reversible aggregates can also cause problems in the ability of SEC to separate individual oligomers. The peaks can contain a mixture of multiple oligomers due to a separation process disturbing the equilibrium between association and dissociation of the aggregates. In addition, SEC will usually resolve components differing in conformation, and so it is important to not, e.g., mix a conformationally altered monomer with an aggregate. Also, when separating and analyzing aggregated mAb samples with SEC-MALS, large and sticky aggregates might cause separation and data interpretation problems. The continuous coelution of large aggregates with the other fractions will cause incomplete separation and incorrectly derived parameters, like MWs.[9]

1.4.2 Luminescent external probes

Luminescence-based, noncovalent, extrinsic probes can also be utilized to detect mAb aggregates. They can be widely applied to characterize proteins[40] because they detect changes in the tertiary structures[41]. Hence, a variety of them can be used to detect aggregates and the unfolding behavior of mAbs since, in both events, the conformation of the mAbs is generally altered[42]. The popularity of these probes is based on their high sensitivity and versatility, relatively low cost, and applicability for high-throughput screening[40]. A common factor with the luminescent probes is that their luminescence emission changes significantly upon interaction with an altered protein structure than a native protein or the absence of protein. Different probes can display different selectivities or specificities for different types and sizes of aggregates due to differences in their functions. The noncovalent interactions between the probe and protein can be, e.g., electrostatic or hydrophobic.[40] One of their disadvantage is the possible interference of the probes on the studied processes by promotion or inhibition[40], which will cause inaccurate results. Some probes can also be sensitive toward detergents, which can hamper their functions. In addition, luminescent probes are not specific only for mAb aggregates but can also probe generally altered protein structures.[43] This can be

considered a disadvantage with the probes since it is not likely that a sample only contains native and aggregated mAb due to the complicated formation of aggregates, but also other altered protein structures.

Commonly used luminescent probes for aggregate detection are organic fluorophores. Characteristic electronic transitions for these molecules are simplified in *Figure 3*. The excitation of a fluorophore causes electrons to move from the ground state S_0 to singlet excited states. After this, various processes can occur as the molecule returns to the ground state and releases the absorbed energy. These processes are internal conversion and vibrational relaxation (*Figure 3a)*), intramolecular charge transfer and solvent relaxation (*Figure 3b)*), intersystem crossing to a triplet state, and luminescence (*Figure 3c)*). All the other processes compete with luminescence and cause a Stokes shift as energy is lost in the other processes. Luminescence is denoted as fluorescence when the molecule relaxes from a singlet excited state, e.g., from S_1 or $S_{(T)ICT}$, to a singlet ground state S_0, where radiationless internal conversion competes with it. The mechanisms through which many of these probes function and exhibit their luminescence features are based on (twisted) intramolecular charge transfers (TICT, ICT) and solvent relaxation processes following the excitation of the molecules.[40] The solvent polarity plays a crucial role in solvent relaxation processes[44]. A change in the dipole moment of the probe usually occurs due to the electronic transitions. Polar solvent molecules might, in response to this, also orient in an energetically more favorable position. This, in turn, will cause a larger Stokes shift due to a smaller energy difference between the energy levels of S_0 and S_1. On the other hand, in intramolecular charge transfer, an electron is transferred from an electron-donating group to an electron-withdrawing group inside the probe molecule. E.g., aromatic systems can act as electron-withdrawing groups while amino groups are good electron-donating groups. In the case of a twisted intramolecular charge transfer, a change in the conformation of the probe must occur for the charge transfer to take place. Luminescent molecules that can form twisted states upon excitation are frequently called molecular rotors. The dipole moment in the $S_{(T)ICT}$ will be enhanced due to the charge transfer, and this will, in turn, increase solvent relaxation processes.[40] A benefit with probes relaxing through intramolecular charge transfer is that from these energy states, the relaxation is often non-luminescent, meaning that they will have low luminescence in polar solvents[45]. As the environment changes or interactions with proteins occur, the relaxation pathways are altered. This can be seen as a change in the luminescence intensity and a possible change in the emission peak maximum.[40]
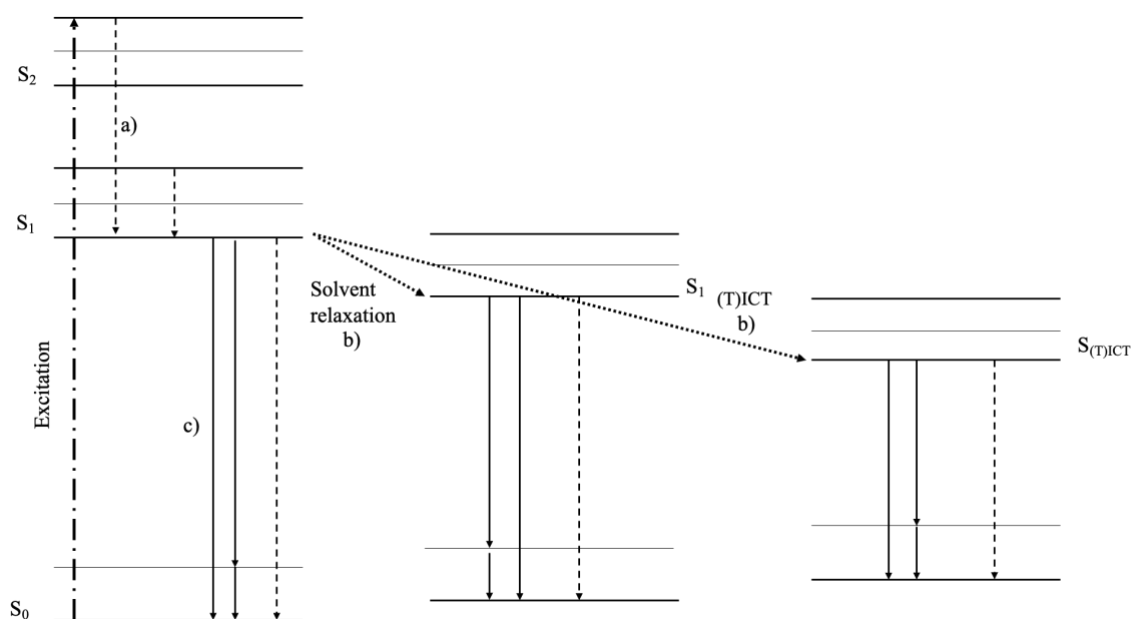
Figure 3. A scheme illustrating different energy levels and electronic transitions characteristic for organic fluorophores. The dashed dotted line represents the light absorption and excitation of electrons. Absorption to only one excited state of S_2 is shown for a more simplified presentation. After excitation, different relaxation processes can occur: a) radiationless vibrational relaxation and internal conversion processes (dashed arrows), b) solvent relaxation and (twisted) intramolecular charge transfer (T)ICT (dotted arrows) and c) luminescence (solid arrows). A possible conversion to the triplet state is not shown in this figure. The figure is adapted from Hawe, A., *et al.*, *Pharm. Res.* **2008**, *25*, 1487–1499.

Resonance Energy Transfer (RET) implementations measure distances between two points between 15-100 Å from each other. This allows a near-Ångstrom resolution, detecting even the slightest conformational changes in, e.g., proteins. Due to this, luminescent probes that utilize RET are effective for studying mAb aggregation. For example, a Eu^{3+}-chelate can be utilized as a donor fluorophore that transfers the energy to an acceptor fluorophore. The excitement of the donor results in an oscillating electric dipole field, which interacts with the energy levels of the acceptor. The transfer of energy is dependent on the distance R between the donor and acceptor, and it decays as R^{-6} when $R << \lambda$ (wavelength of donor emission). In addition to the distance between the donor and acceptor, also spectral overlap is required for the energy transfer.[46] Utilizing a Eu^{3+}-chelate as the donor in RET applications has many benefits, like sharp and defined emission peaks. The excitation of the antenna occurs in the ultraviolet region (340 nm) and the emission of the Eu^{3+}-ion the red of the visible spectrum (615 nm), which results in a large Stokes shift.[46] In addition, a Eu^{3+}-chelate enables time-resolved luminescence (TRL) measurements, where a lag time is used before the emission is read. This reduces the background signal and allows higher sensitivity[47]. TRL measurements can be utilized

since the emission lifetime of Eu^{3+}-chelate is in the millisecond region[46]. *Figure 4.* is a simplified scheme of the electronic transitions taking place in a RET application with a Eu^{3+}-chelate as the donor molecule. The organic chelate surrounding the Eu^{3+}-ion offers protection from water and transfers the absorbed energy from the antenna[46]. Intersystem crossing in the chelate from S_1 to the triplet state T_1 (*Figure 4a)*) is followed by intramolecular energy transfer to the Eu^{3+}-ion (*Figure 4b)*)[48]. The long emission lifetime obtained with the Eu^{3+}-chelate is due to forbidden electronic transitions between 4f energy levels of the Eu^{3+}-ion[46]. Lastly, the energy is transferred to the acceptor via RET (*Figure 4c)*).
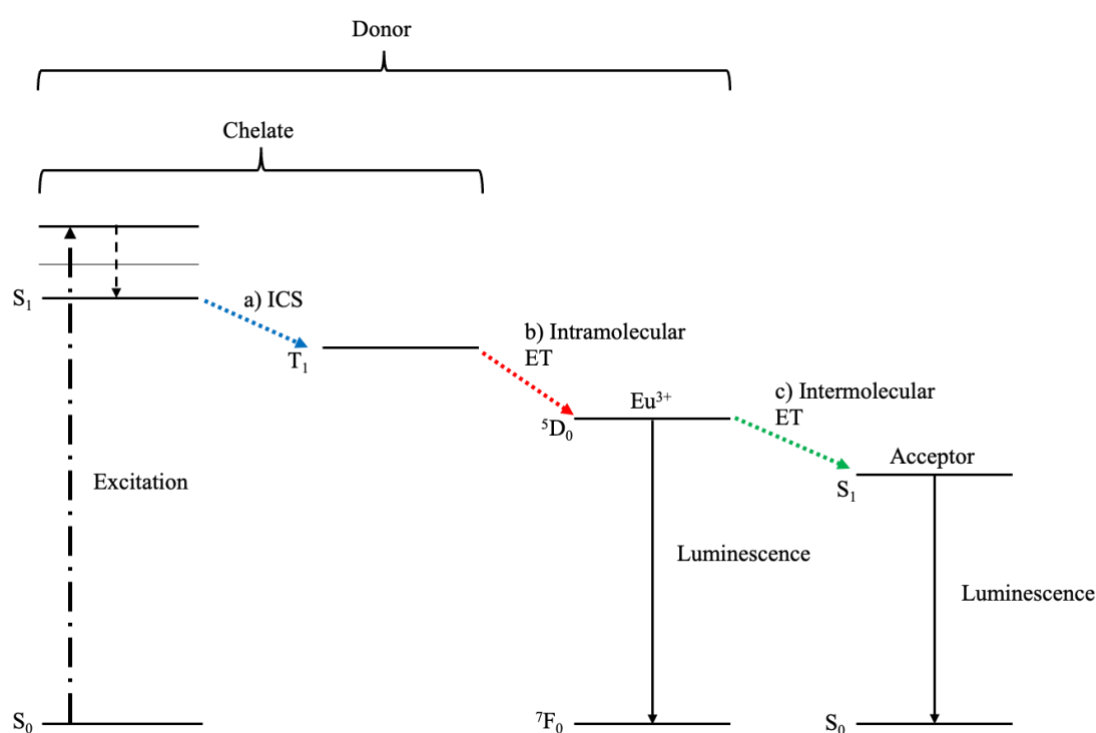

Figure 4. A simplified Jablonski diagram representing the electronic transitions taking place in a RET application that utilizes a Eu^{3+}-chelate as the donor. After excitation of the chelate structure from S_0 to S_1, a) intersystem crossing (ISC, dotted blue arrow) to a triplet state T_1 inside the chelate takes place. After this, b) an intramolecular energy transfer (ET, dotted red line) from the chelate to the Eu^{3+}-ion occurs. Lastly, c) an intermolecular energy transfer (ET, dotted green line) to the acceptor can occur. Dashed arrow = radiationless vibrational relaxation and internal conversion processes.

8-Anilino-1-naphthalenesulfonate (ANS) (*Figure 5a)*) is a luminescent probe that has been in use for protein characterization for decades. The probe is excited at approximately 370 nm, and it has an emission maximum of 500 nm. The luminescence properties of ANS are sensitive to changes in its environment, e.g., polarity and viscosity.[40] As the dielectric constant of the solvent decreases, a blue shift and an increase in the quantum yield of luminescence occurs[49]. The amino and naphthalene structures in ANS (*Figure*

5a)) promote TICT in polar environments, resulting in low luminescence[45]. In general, interactions with proteins change the polarity and viscosity of the environment, which reduces the relaxation of the probe through solvent relaxation processes, and TICT, which changes the luminescence properties of the probe[40]. The main interactions through which ANS binds to proteins are hydrophobic and electrostatic. The negatively charged sulfonate groups create ion pairs with the positively charged amino acids[50].

SYPRO Orange is a zwitterionic merocyanine probe (*Figure 5b)*) popular for probing protein structures. It has an excitation maximum of approximately 470 nm and an emission maximum of 570 nm. The excited state of SYPRO Orange is highly polar due to the intramolecular charge transfer between the dimethylaniline group and the pyridinium (*Figure 5b)*). In polar solvents, the quantum yield of the emission decreases, which indicates that non-radiative relaxation from the excited state is promoted. In addition to solvent polarity, also viscosity affects the luminescence properties of the probe. An increase in emission quantum yield is proportional to the viscosity of the solvent. This relationship can be explained by the large amplitude diffusional motion, e.g., twisting of the molecule, hindered in high viscosity, so luminescence is favored instead of non-radiative decay pathways. It has been suggested that SYPRO Orange acts like a molecular rotor and that the emission properties of the probe are highly dependent on the solvent viscosity[51]. Despite this, it is generally considered a hydrophobic probe like ANS. At low protein aggregate concentration, the probe mainly binds the aggregates by hydrophobic interactions, but at higher aggregate concentrations, also hydrogen bonding takes place with the amino acids.[51]

ProteoStat is a luminescent rotor probe with a structure based on Thioflavin T[52] (*Figure 5c)*), a probe used to detect amyloid fibrils. The probe has an excitation maximum of 550 nm and an emission maximum of 600 nm. The detection of aggregates is based on the rotation of the probe around a single bond. While freely rotating in a solution free of suitable binding pockets or at low viscosity, the luminescence intensity of the molecule is negligible. In a solution containing aggregates, the probe binds to them, which in turn prevents the free rotation and results in high luminescence intensity.[43]
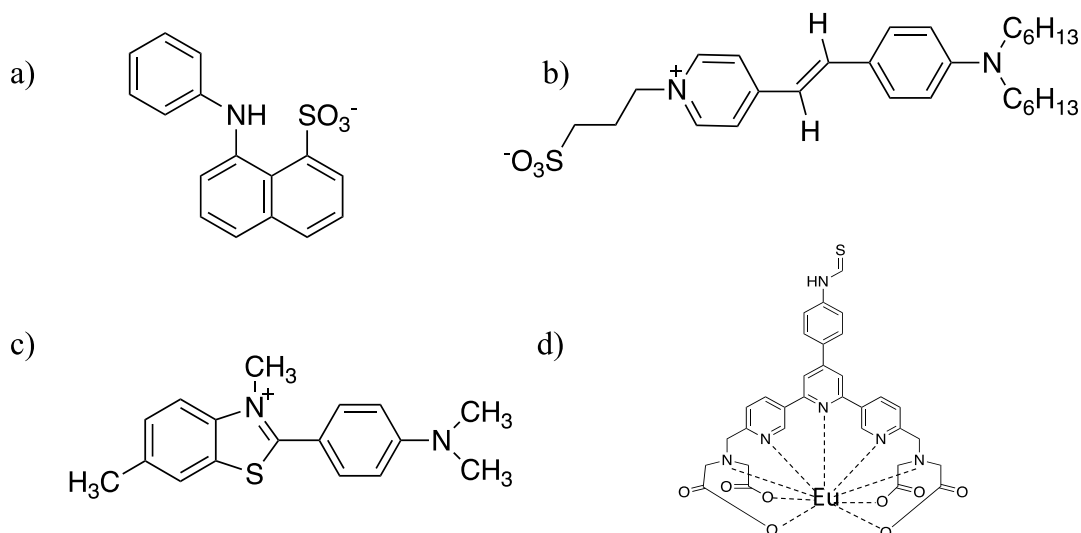
Figure 5. The chemical structures of a) ANS, b) SYPRO Orange, c) Thioflavin T, and d) Eu^{3+}-chelate.

The Protein-Probe and TR-FRET –methods utilize a Eu^{3+}-chelate (*Figure 5d)*), conjugated to a negatively charged probing peptide[53]. This conjugate is referred to as Eu^{3+}-probe. In addition, both methods are based on RET, so an additional fluorophore is included. The Protein-Probe method utilizes a soluble quencher, which absorbs at the main emission peak of 616 nm of the Eu^{3+}-chelate and acts as an acceptor in the energy transfer. The Eu^{3+}-probe has little interaction with native mAbs, but as they form aggregates, the reveal of hydrophobic areas leads to interactions between the aggregates and the probe. These interactions reduce the quenching effect of the quencher and so lead to an increase in the (TRL) signal.[53] The basic function of the Protein-Probe is presented in *Figure 6a)*.

The TR-FRET (Time-resolved fluorescence resonance energy transfer) method utilizes a FRET-probe comprising of a similar Eu^{3+}-probe with the acceptor conjugated to the structure. In the absence of, e.g., heat-denatured and aggregated mAbs, the distance between the donor and the acceptor is too long for any energy transfer and subsequent emission from the acceptor to occur. As hydrophobic patches are revealed, the peptide connecting the Eu^{3+}-chelate and the acceptor interacts with the mAbs. The process brings the donor and acceptor close enough for the Eu^{3+}-chelate to transfer its energy to the acceptor. As a result, the acceptor emission is the indicator of FRET-probe-antibody interaction, and the signal increases in proportion to the interactions. The basic function of the FRET-Probe is presented in *Figure 6b)*.
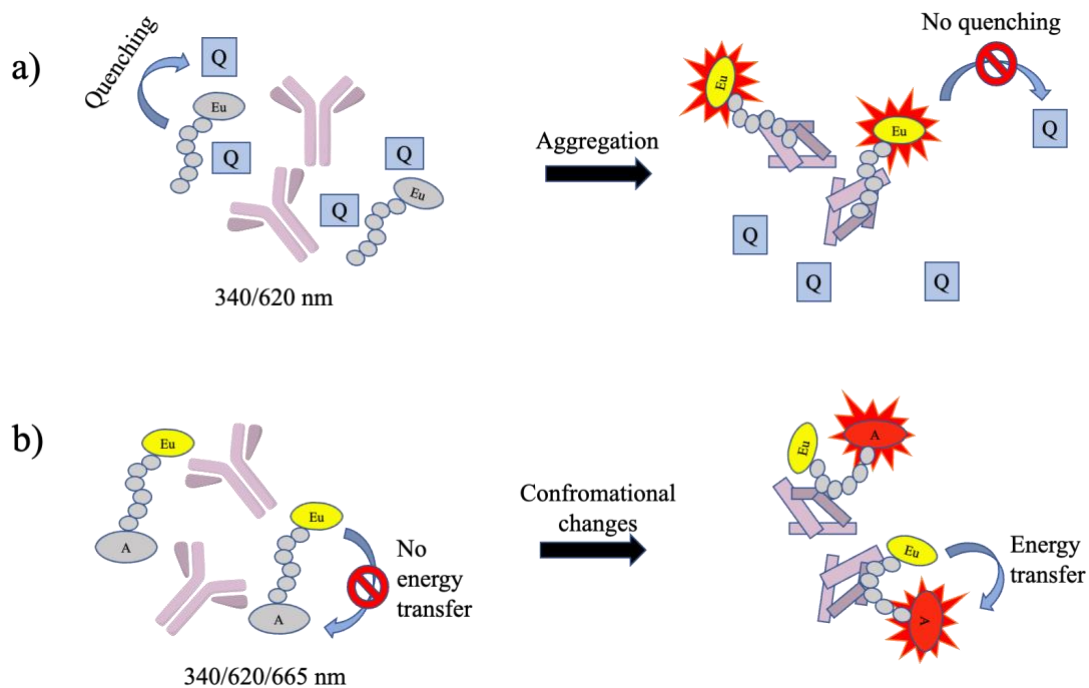
Figure 6. A schematic illustration of the basic function of a) Protein-Probe and b) FRET-probe in the detection of mAb aggregates or conformationally altered mAbs. Q = quencher (also acceptor), A = acceptor.

2 Experimental section

2.1 Materials

0.2 μm Syringe Filter, Hydrophilic PTFE (Millex); 384 well skirted PCR plate (FrameStar); ANS (Alfa Aesar); Antibody X mIgG1 (Orion Corporation); Atezolizumab mIgG2a (Icosagen); Bococizumab hIgG1 (Orion Corporation); CellCarrier-96 ultra black (PerkinElmer); Citric acid monohydrate (Sigma-Aldrich); Na_2HPO_4 (Merck); Optiplate-384 black well plates (PerkinElmer); PBS 1X, 10X (Gibco, Lonza); Pembrolizumab hIgG1 (Icosagen); Protein-Probe-kit (QRET Technologies); FRET-probe (In-house, under development); Proteostat aggregation assay kit (Enzo Life Sciences); Proteostat aggregation-% standards (Enzo Life Sciences); Slide-A-Lyzer™ MINI Dialysis Device 3.5K MWCO, 0.5 mL (Thermo Fisher Scientific); Slide-A-Lyzer™Dialysis Cassettes G2 3.5K MWCO, 3 mL (Thermo Fisher Scientific); SYPRO Orange (Sigma-Aldrich); Trastuzumab hIgG1 (Roche); Triton X-100 (Honeywell).

2.2 Instrumentation

Size-exclusion chromatography was performed using Agilent 1260 Infinity II LC Bio-inert System with Agilent 1260 Infinity II Diode Array Detector WR combined with

17

Wyatt miniDAWN MALS and Optilab instrumentations and WyattQELS module. AdvanceBio SEC 300A column (Agilent Technologies) was used with AdvanceBio SEC 300A guard column (Agilent Technologies). 1xPBS was used as the eluent in all the analyses, and 20 µg of samples were injected as duplicates. The employed flow rate was 0.350 ml/min. The data were analyzed using ASTRA software (Wyatt Technology).

NanoDSF and batch mode DLS were measured with Prometheus Panta -instrumentation (NanoTemper Technologies). The used excitation power in each nanoDSF measurement was determined using the autodetection feature. The used temperature ramp in nanoDSF was 1 °C/min from 20 °C to 95 °C. The samples were excited using a wavelength of 280 nm, and the luminescence at 330 nm and 350 nm was recorded to obtain 350/330 nm used in data analysis. The laser intensity used in the DLS measurements was 100 % with a temperature of 25 °C. All the obtained information was derived from the Panta Control Software (NanoTemper Technologies).

The aggregation samples were measured with Envision Multimode Plate Reader (PerkinElmer), and the thermal unfolding of the mAbs was monitored with Tecan Spark 20M (Tecan Life Sciences). The excitation and emission wavelengths used for Protein-Probe, FRET-probe, ProteoStat, SYRO Orange, and ANS were 320/615 nm, 340/665 nm, 510/600 nm, 485/590 nm, and 350/490 nm, respectively. With Protein-Probe and FRET-probe, the TRL signals were measured with a lag and integration time of 800/400 µs and 50/100 µs.

2.3   Methods

2.3.1   Luminescent probes for aggregate detection

With Protein-Probe and ProteoStat, the detection solutions were prepared according to the instructions provided by the manufacturers. With SYPRO Orange, the detection solution was prepared by diluting the stock (5000X) with MQ-H_2O to obtain a final concentration of 5x in the wells. The detection solution volume to sample volume used with Protein-Probe, ProteoStat, and SYPRO Orange were 65/2 µl, 2/98 µl, and 2/28 µl, respectively. With Protein Probe and SYPRO Orange, a black, flat-bottomed 384-well plate was used, while with ProteoStat, the measurements were performed on a clear-bottomed 96-well plate. In the Protein-Probe assay, the plate was shaken for 10 seconds and incubated for 1 hour in the dark before measurement. With ProteoStat, the incubation time was 15 min.

2.3.2 Dialyzing trastuzumab

Trastuzumab was used as a model antibody, and to obtain more comparable results, it was dialyzed against MQ-H_2O to remove excipients used for storage. This was done by using 3 ml 3.5K MWCO dialysis chambers (Thermo Fisher Scientific). The dialysis was done at 4 °C by changing the MQ-H_2O three times before dialyzed overnight.

2.3.3 Thermal unfolding

The thermal unfolding curves of the five studied antibodies were measured and compared using nanoDSF, FRET-probe, SYPRO Orange, and ANS. The trastuzumab analyzed with the FRET-probe was in the commercial formulation. For the FRET-probe, the antibodies were diluted in 0.1xPBS, while 1xPBS was used with SYPRO Orange and ANS. The final mAb concentrations in the wells were 0.004 mg/ml with Protein-Probe, and 0.5 mg/ml with SYPRO Orange and ANS. With FRET-probe, the samples were analyzed as n = 4, while n = 3 was used with SYPRO Orange and ANS. For the detection solutions, SYPRO Orange and ANS were diluted with 1xPBS to obtain final concentrations of 5x for SYPRO Orange and 10 µM for ANS in the wells. In addition, the detection solutions contained 0.0008 % of Triton X-100 in the final well volumes. With SYPRO Orange and ANS, 20 µl of the sample was used with 5 µl of detection solution. For the FRET-probe, the detection solution was prepared by diluting the probe in 0.1xPBS to obtain a dilution of 1/2000 in the wells. Additionally, the detection solution contained 0.008 % of Triton X-100 in the final well volumes. With the FRET-probe, 5 µl of the sample was used with 20 µl of detection solution.

With all the external probes, a black 384-well PCR plate was used. Following the addition of all the components, the plates were incubated for 10 seconds on a plate shaker. After this, the luminescence signals were read at the set wavelengths first at room temperature. A PCR machine (PTC-200, MJ Research) was used to heat the samples. The mAbs were heated at 50–88 °C using 2 min measurement interval every 2 degrees. For the nanoDSF measurements, the mAbs were diluted to 1 mg/ml with 1xPBS containing 0.0008 % of Triton X-100. The samples were analyzed as n = 3. The melting curves and the derived parameters were obtained by the Panta Control software (NanoTemper Technologies).

The T_m-values were calculated by fitting the data with standard sigmoidal fitting functions with Origin 2016 (OriginLab). For multiple unfolding events, a sigmoidal function was fit independently. In addition, some data points were removed to obtain the best fit possible and subsequently derive accurate T_m-values. The lower limit of detection (LLD)

for each external probe was calculated based on the signal-to-background-ratio (S/B) of trastuzumab in each method's optimized concentration. The lower limit of detection was calculated as LLD = $c/S/B/5$, where c = concentration of trastuzumab used with each method and S/B = the highest S/B-ratio of the measurement. The sensitivities of the methods were further studied by using trastuzumab as a model antibody at the concentration of 0.01 mg/ml.

2.3.4 Proteostat and self-produced aggregation-% standards

The Proteostat aggregation-% standards were used with the well plate –based methods to evaluate the aggregation-% of the samples. Additional 0.1 % and 0.05 % standards were produced by diluting the 12.5 % standard with the 0 % standard. In addition, self-produced, aggregated trastuzumab (AT) standards were produced. The standard curves were produced by fitting the data with linear fitting functions with Origin 2016 (OriginLab). The LLD for each probe using both standard curves were calculated as $y = 3 * SD(background(0\% \, standard))$, where SD = Standard Deviation. The signals obtained from different experiments were normalized to these standard curves with five same standard samples, if not stated otherwise, to obtain the aggregation-%s. Diverging from the SYPRO Orange protocol, an hour of incubation time was needed for the AT standards to obtain acceptable SD within the standards. The two standard sets were also analyzed with SEC-MALS and DLS. Before the analysis of the standards with SEC-MALS, the samples were centrifuged to prevent column blockage. The samples were centrifuged with 14 000 G for 10 min at 4 °C.

The AT standards were prepared by diluting trastuzumab with 1xPBS to create a 1 mg/ml solution. A part of this solution was fully aggregated by incubation at 85 °C for 3 min, which was used to spike the monomeric solution to create the standards[53]. The same aggregation-% standards were produced than in the Proteostat Aggregation-% Standards kit: 1:2 dilution series from 12.5 % to 0.2 %. In addition, the two aggregation standards containing lower amounts of aggregates of 0.1 % and 0.05 % were produced.

2.3.5 Long-term incubation of trastuzumab and atezolizumab at elevated temperatures

2 mg/ml trastuzumab and atezolizumab were heated using heating blocks. Trastuzumab was incubated at 57 °C and atezolizumab at 53 °C. Samples were collected daily, and the collection included diluting the antibodies to 1 mg/ml using 1xPBS and placing them at 4 °C until simultaneous analysis. Protein-Probe was used as a follow-up method to monitor the level of aggregation in the samples daily. Samples were collected on days 1,

2, 3, 4, 7, 9, and 11, after which they were analyzed using DLS, Protein-Probe, and ProteoStat. The background used in the background reduced signals was the signal of the unstressed, native antibody.

2.3.6 Short-term incubation of mAbs at elevated temperatures

A rapid aggregation protocol was conducted by heating all the studied antibodies at 60 °C and 70 °C for short periods. 0.2 mg/ml of trastuzumab, atezolizumab, bococizumab, pembrolizumab and antibody X solutions were used. A lower mAb concentration was used in this experiment due to high sample consumption. The samples were divided into three different pools. Two pools were aggregated at the used temperatures, while the third one was used as a reference for the native mAb. Both aggregated pools were incubated at the chosen temperatures for 10 min. After this, all the samples were analyzed using SEC-MALS, DLS, Protein-Probe, SYPRO Orange, and ProteoStat. For SEC-MALS, the samples were centrifuged prior to the analysis with 14 000 G for 10 minutes at 4°C.

2.3.7 Low pH incubation of trastuzumab, atezolizumab and pembrolizumab

0.1 M citric acid and 0.2 M Na_2HPO_4 were used to create citric acid – Na_2HPO_4 buffer in pH 3.2, 3.6, and 6.0. 1 mg/ml of trastuzumab, atezolizumab, and pembrolizumab were divided into three different pools: one was dialyzed in pH 3.2, one in pH 3.6, and one, used as a reference, was stored at 4 °C. The other two pools per mAb were placed in the low pH buffers heated to 37 °C using 0.5 ml dialysis chambers with 3.5K MWCO (Thermo Fisher Scientific). The samples were dialyzed in pH 3.2 and 3.6 for 3 hours while stirring at 100 rpm. After 3 hours, the samples were transferred in the same dialysis chambers into the pH 6.0 citric acid – Na_2HPO_4 buffer. The samples were dialyzed in the pH 6.0 buffer at 4 °C overnight while stirring at 100 rpm. The buffer volume was 417x greater than the total sample volumes in all the dialysis steps.

Dialysis caused slight mAb concentration dilution, and thus all samples were diluted to the lowest concentration in the sample set. The native reference samples were diluted with 1xPBS, while the aggregated samples were diluted with the pH 6.0 citric acid – Na_2HPO_4 buffer. The concentrations after the dilutions for trastuzumab, atezolizumab and pembrolizumab samples were 0.86 mg/ml, 0.92 mg/ml, and 0.84 mg/ml, respectively. Subsequently, all the samples were analyzed using SEC-MALS, DLS, Protein-Probe, SYPRO Orange, and ProteoStat. Before injecting the samples into SEC, they were filtered with a 0.2 μm syringe filter.

3 Results and discussion

3.1 Thermal unfolding studies with nanoDSF, SYPRO Orange, ANS and FRET-probe methods

The melting curves of all the mAbs derived by (nano)DSF -methods are presented in *Figure 7*. For many mAbs, the probes exhibited noticeably higher luminescence signals at room temperature than at higher non-denaturation temperatures. This has been hypothesized to be due to a degree of aggregation[53] in the native mAb formulation. It could also indicate specific interactions between the probe and the native mAb structure independent of aggregation. For trastuzumab, two phases were detected with SYPRO Orange, FRET-probe and, nanoDSF, indicative of the unfolding of different mAb domains/regions. In addition, nanoDSF detected two unfolding events for bococizumab while the external probes detected only one. This could suggest that intrinsic luminescence is more sensitive than the external probes in detecting domain/region-dependent unfolding. Also, the different transitions were the most distinguishable when produced with intrinsic luminescence. However, the number of transitions detected with each method is also mAb-dependable, and the amount of tryptophan residues or secondary structures affects the results. For atezolizumab and antibody X, ANS and SYPRO Orange presented seemingly a second transition after the first one, but these are most likely artifacts since the methods are not very specific.

The T_m-values obtained for the mAbs with each method are presented in *Table 1*. For trastuzumab, ANS seemed to result in a higher transition temperature near 80 °C. High SDs obtained with the probes for the last data points were most likely due to evaporation at high temperatures. The two T_m-values obtained with FRET-probe and nanoDSF are similar, while SYPRO Orange yielded lower transition temperatures. Similar T_m-values have been previously reported for trastuzumab with nanoDSF (70 °C and 80 °C)[54]. The first unfolding transition is likely due to the CH2 domain, and the second is due to the Fab and/or CH3[25]. Some variance occurred with the T_m-values obtained with the different methods. The largest discrepancy between the methods occurred for bococizumab (*Figure 7d)*). The first unfolding event was detected at approximately 62 °C, 63 °C, 57 °C, and 70 °C with nanoDSF, FRET-probe, SYPRO Orange, and ANS, respectively. The second unfolding event detected with nanoDSF occurred at around 76 °C. Interestingly, the T_m-value obtained with ANS was between the two values obtained with nanoDSF. It

may indicate that ANS detected the two unfolding events as one transition. Differences in T_m-values were expected since the used mAb concentrations and conditions varied between the methods. Overall, the obtained T_m-values were relatively uniform, except for SYPRO Orange producing slightly lower values than the other methods. Additionally, the Tm-value of trastuzumab derived with ANS deviated from the other probes.

The external probes interacted differently with different mAbs, and this caused variation in the mAb detectability. ANS exhibited high SD and low S/B-ratio for antibody X. This may indicate that the interactions between antibody X and ANS upon the unfolding process are suboptimal, and the studied unfolding event is difficult to detect. SYPRO Orange did not seem to bind antibody X at lower temperatures, while ANS and the FRET-probe had significant interactions with the mAb prior to the unfolding event. The curves created for pembrolizumab did not suffer from the above-mentioned and were uniform between the methods. Bococizumab exhibited the most deviating unfolding curve with most of the methods. With nanoDSF, a large decrease in 350/330 nm was observed at the beginning of the heating. This indicates that the heating initially caused an increase in hydrophobicity around the luminescent amino acid residues. At temperatures around 55°C, the 350/330 nm increased, indicating that the luminescent residues were exposed to a more hydrophilic environment. Also, ANS and the FRET-probe exhibited relatively high luminescence already at RT for bococizumab.
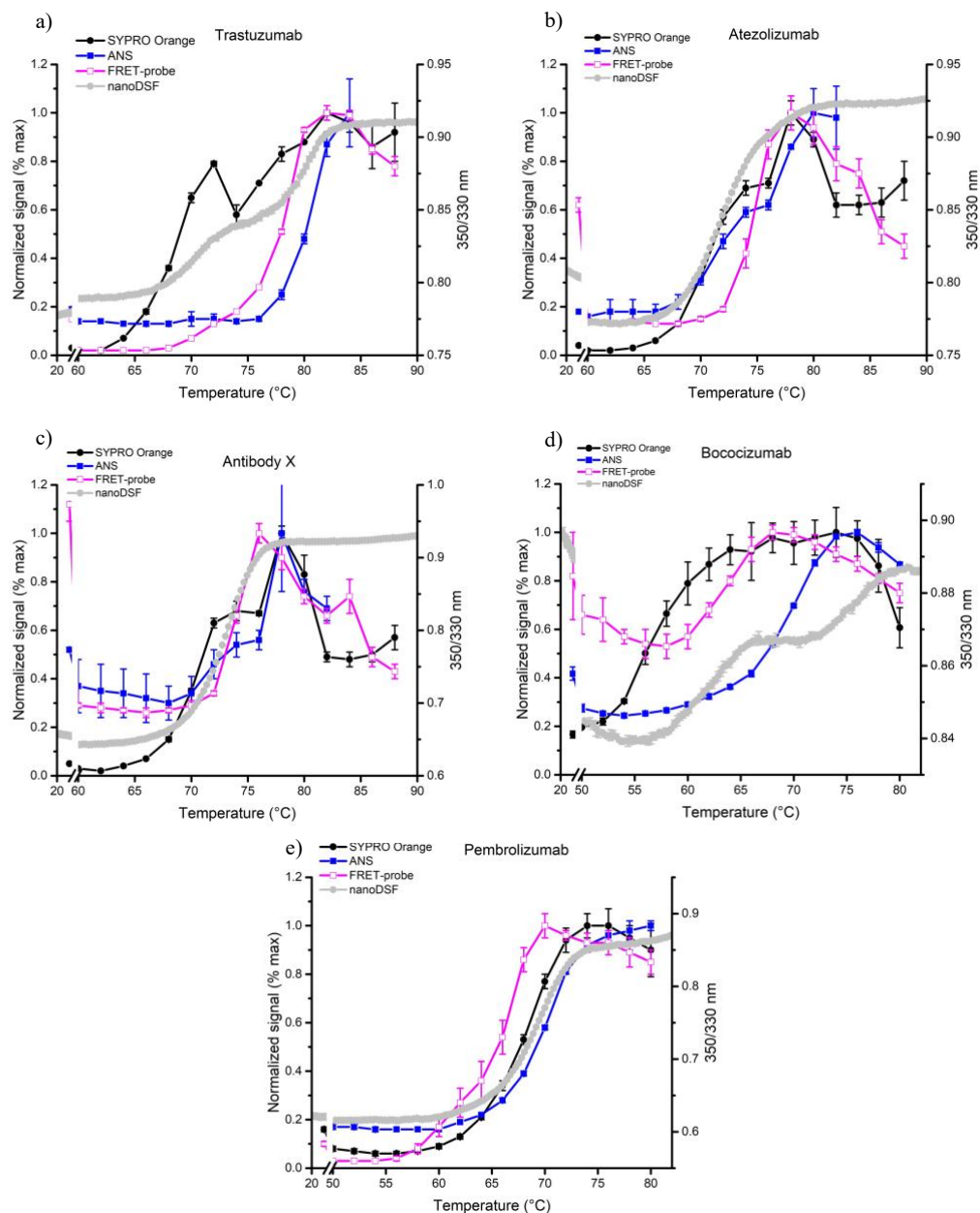
Figure 7. The melting curves of a) trastuzumab, b) atezolizumab, c) antibody X, d) bococizumab and e) pembrolizumab obtained with the (nano)DSF methods. The luminescence signal from the external probes has been normalized against the highest signal and the data from nanoDSF is presented as 350/330 nm.

Table 1. The T_m-values obtained with different methods for the studied mAbs.

Tm(s) (°C)	SYPRO Orange	ANS	FRET-probe	nanoDSF
Trastuzumab	$68.6 \pm 0.3; 76.3 \pm 1.7$	80.5 ± 0.1	$71.4 \pm 0.2; 78.3 \pm 0.2$	$70.3 \pm 0.1; 79.8 \pm 0.1$
Atezolizumab	70.4 ± 0.1	71.2 ± 0.1	74.6 ± 0.1	72.1 ± 0.1
Antibody X	70.0 ± 0.2	71.8 ± 0.3	74.1 ± 0.1	72.8 ± 0.1
Bococizumab	56.9 ± 0.2	69.6 ± 0.3	63.4 ± 0.2	$61.7 \pm 0.1; 75.5 \pm 0.1$
Pembrolizumab	68.1 ± 0.2	69.9 ± 0.2	66.1 ± 0.4	69.2 ± 0.1

The S/B-ratios and the LLDs of the external probes are presented in *Table 2*. Compared to the other methods, SYPRO Orange had high S/Bs for all the studied mAbs, while ANS provided the lowest S/B-ratios in the experiments. On the other hand, FRET-probe

showed the most variance in the S/B-ratios between different mAbs. These values are not reported for nanoDSF, as they are not fully comparable. In terms of sensitivity, the methods varied greatly. The LLDs were calculated as c/S/B/5, where c = concentration of trastuzumab used with each method (*Table 3.*) and S/B = the largest signal-to-background-ratio of the measurement. The FRET-probe had the lowest LLD of 0.013 µg/ml, while ANS had the largest of the three (13 µg/ml). The concentration range for the nanoDSF instrument provided by the manufacturer is 5 µg/mL – 250 mg/mL. Hence, it can be deduced that nanoDSF has a similar sensitivity to SYPRO Orange.

Table 2. The S/B-ratios obtained for the studied mAbs and the LLD for trastuzumab calculated for each external probe.

S/B	SYPRO Orange	ANS	FRET-probe
Trastuzumab	45	7.6	64
Atezolizumab	36	3.7	8
Antibody X	28	1.8	3.8
Bococizumab	5.6	4.1	1.9
Pembrolizumab	16	6.1	39
LLD (µg/ml)			
Trastuzumab	2.2 ± 0.1	13 ± 0.1	0.013 ± 0.001

Table 3. The protocols optimized for each (nano)DSF method and used in the thermal unfolding experiments.

Thermal unfolding protocols	SYPRO Orange	ANS	FRET-probe	nanoDSF
MAb concentration (mg/ml)	0.5	0.5	0.004	1
Buffer	PBS (1x)	PBS (1x)	PBS (0.1x)	PBS (1x)
Triton X-100 (%)	0.0008	0.0008	0.008	0.0008
Sample volume (µl)	20	20	5	10
Total volume (µl)	25	25	25	10

The sensitivities of the methods were further examined by producing thermal profiles for trastuzumab at a concentration of 0.01 mg/ml (*Figure 8.*). Per the calculated LLDs, ANS could not produce an unfolding curve for trastuzumab at the given concentration. While SYPRO Orange and nanoDSF could produce unfolding curves at this concentration, the curves were not as well defined as with an optimized trastuzumab concentration (*Figure 7a*)). SYPRO Orange detected the first unfolding transition clearly, but the second transition had disappeared. With nanoDSF, the assay window reduced from approximately 0.1 to 0.04, and as a subsequence, the two transitions were not as distinct anymore. The clear second transition temperature increased by 1.7°C from the previous experiment. The dependency of the Tm-values on concentration has been discovered before. It has been proposed that aggregation masks the correct Tm-values at higher concentrations[53]. The FRET-probe, on the other hand, worked well with this

concentration, which is not surprising since the optimized concentration of the method was 0.004 mg/ml. However, FRET-probe did suffer from higher SD, which could indicate that the concentration is suboptimal.
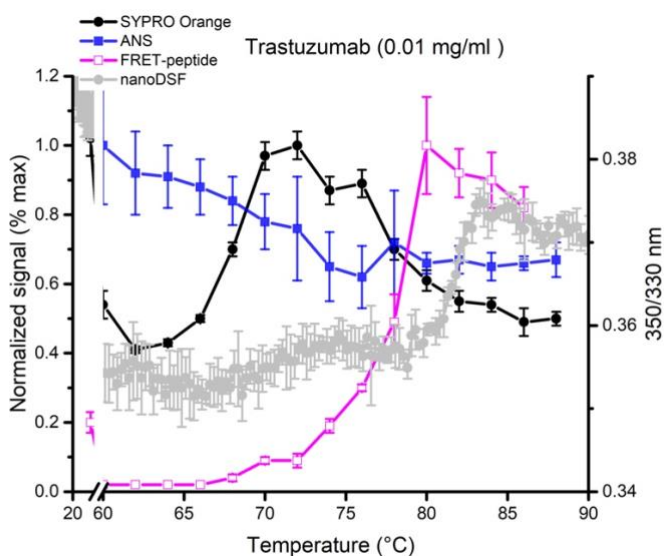

Figure 8. The thermal unfolding curves obtained for 0.01 mg/ml trastuzumab with SYPRO Orange, ANS, FRET-probe and nanoDSF.

3.2 Antibody aggregation-% standard studies with ProteoStat, SYPRO Orange, Protein-Probe, DLS and SEC-MALS

The two sets of aggregation-% standards were analyzed with SYPRO Orange, ProteoStat, and Protein-Probe to create two standard curves for each method, which could be used to quantify the aggregate amount in the samples produced in the aggregation studies. In addition, both sets were analyzed with DLS and SEC-MALS to obtain information on the content and explain possible differences between the aggregate sets. The sample and detection solution volumes required for the used methods are presented in *Table 4*.

Table 4. The sample and detection solution volumes used in the aggregation studies.

Protocols	ProteoStat	SYPRO Orange	Protein-Probe	DLS	SEC-MALS
Sample volume (µl)	98	28	2	10	20–100 (20 µg)
Detection solution volume (µl)	2	2	65	–	–

The standard curves measured with all three probes for the ProteoStat and Aggregated Trastuzumab (AT) aggregation-% standards are presented in *Figure 9*. For the ProteoStat standards, SYPRO Orange could detect the aggregate content from 0.39 % upwards. For ProteoStat, the minimum aggregate content detected was 0.2 %, but this standard did not fit within the linear curve. The standard curves produced with ProteoStat and SYPRO

26

Orange provided similar linear slopes (*Figure 9a)*). With Protein-Probe, two linear fits were necessary, indicating that the probe detected two different phases. This may be due to different types of aggregates in the lower standard concentrations compared to the higher standard concentrations. For ProteoStat, SYPRO Orange and Protein-Probe, the coefficient of variation % (CV %) varied between 0.68 %–13 %, 2.0 %–20 % and 4.3 %–18 %, respectively.

In the production of the AT standards, the fully aggregated sample became cloudy after incubation at 85 °C, indicating large aggregates. The ProteoStat and Protein-Probe methods measured two phases with the given AT standards, but it was more prominent with the Protein-Probe. Therefore, two linear fittings were applied for both probes to obtain linear curves (*Figure 9b)*). With Protein-Probe, the two curves differed significantly from one another. The data indicates that the Protein-Probe may be more sensitive to the higher standard concentrations than the other methods, as the slope for these standards was shallow. For ProteoStat, the trend was the opposite, as the shallower slope was obtained for the lower standard concentrations. However, the difference in the slopes was not prominent. This result supports previous findings indicating that ProteoStat is more sensitive toward smaller aggregates[43]. The different phases suggest the interaction between the aggregates and the probe changes according to the concentration or that the used concentrations were suboptimal. For ProteoStat, SYPRO Orange, and Protein-Probe, the CV % varied between 0 %–34 %, 2.6–21 %, and 3.2–23 %, respectively.
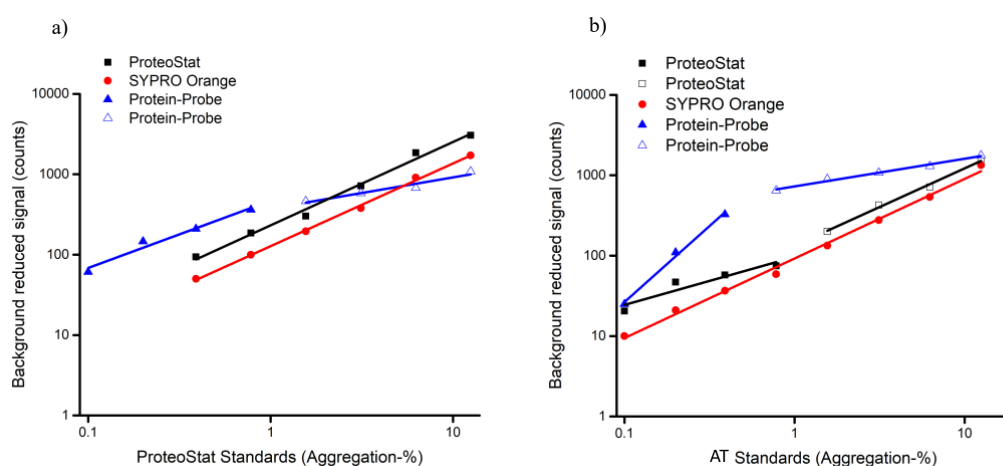

Figure 9. Aggregation-% standard curves created with the probes using a) ProteoStat and b) AT standards.

The LLDs were calculated for the probes with both standard sets as the % aggregate equal to 3xSD of native non-denatured mAb (*Table 5.*). ProteoStat and SYPRO Orange gave similar LLDs at around 0.5 % aggregates with the ProteoStat standards. On the other hand, the Protein-Probe with two slope values gave LLDs of 0.07 % and 0.006 % based on the ProteoStat standards. The steeper curve with an LLD of 0.07 % was used in the aggregation studies as the ProteoStat standard curve to determine the aggregation-% of the samples. The samples were diluted differently for each assay which may affect the outcome and thus must be carefully considered. No dilution in the wells occurred in the ProteoStat and SYPRO Orange assays, while with Protein-Probe, the dilution factor was 33.5 (*Table 4.*). Therefore, the total concentration of aggregates in the Protein-Probe method was significantly lower. For example, with the 1.56 % standard, the actual aggregate concentration in the Protein-Probe assay is 0.05 %.

With the AT standards, two LLDs were obtained for Protein-Probe and ProteoStat. For ProteoStat, the two LLDs of 0.61 % and 0.53 % did not differ significantly (*Table 5.*). Altogether, the LLDs calculated from both standard sets with the ProteoStat-probe were in good accordance. The two LLDs obtained for Protein-Probe were again quite different. The first LLD of 0.063 % was in good agreement with the LLD obtained with the ProteoStat standards, while the second LLD of 0.001 % was significantly lower. The lower LLD is inaccurate and could be due to the low number of replicates used. With Protein-Probe and ProteoStat, the curves with an LLD of 0.063 % and 0.53 % were used in the aggregation studies as the standard curves to determine the aggregation-% of the samples. SYPRO Orange had over 2x improved LLD of 0.21 % for the AT standards than ProteoStat standards.

Protein-Probe and ProteoStat interacted differently with the two standard sets, while with SYPRO Orange, this was not prominent. This could result from different aggregate binding specificities, which result in varying selectivities. Protein-Probe is possibly more sensitive at probing minimal structural changes than the other probes. It could also be deduced that SYPRO Orange is the least specific since it produced only one standard curve with both standard sets and did not differentiate between the standards. The lowest LLD was obtained for the Protein-Probe with both standard sets.

Table 5. LLD in % aggregates for each method based on the ProteoStat and AT standards.

LLD: % aggregates	ProteoStat	SYPRO Orange	Protein-Probe
ProteoStat standards	0.53 ± 0.02	0.57 ± 0.01	0.070 ± 0.009;0.006 ± 0.004
AT standards	0.61 ± 0.02;0.53 ± 0.01	0.21 ± 0.02	0.063 ± 0.004;0.001 ± 0.001

Analyzing two standard sets with DLS resulted in the size distributions shown in *Figure 10*. DLS detected only the presumed monomer peak with all the ProteoStat standards (*Figure 10a)*). A slight variation in the monomer peak intensity was detected, but it did not follow the decreasing aggregate content. For the standards with lower aggregate concentration, the r_H was approximately 6.2 nm. With increasing aggregate content, the r_H of the monomer peak decreased, and for the 12.5 % standard, it was 5.8 nm. For all standards except one, the polydispersity index (PDI) of the main peak was below 0.2. While this indicates that the standards are not fully homogeneous, a PDI below 0.2 is considered an acceptable limit for a sufficiently homogeneous sample. Without knowledge of the buffer used in the ProteoStat standards, it was set as PBS. If inaccurate, it might have affected these results.

The size distributions for the 0, 0.05, and 0.1 % standards were nearly identical for the AT standards. A noticeable decrease in the monomer peak frequency occurred in the standards with 0.78 % aggregates or more (*Figure 10b)*). The monomer peaks shifted and widened when the aggregate content increased to 1.56 % or more, which also caused the particle sizes and the PDIs to increase. The r_H of the monomer peak was approximately 5.7 nm for the lower standard concentrations but increased up to 7.8 nm for the 12.5 % standard. For the standards of 6.25 and 12.5 %, the PDI of the monomer peak was significantly over 0.2. Thus, DLS was not able to separate the contents in these peaks. In addition, a peak at around 30 nm was prominent with the 6.25 and 12.5 % standards. By decreasing the relative frequency scale, particles above 1 μm became more visible (*Figure 10c)*). The 12.5, 6.25, and 3.13 % standards seemed to have particles in the μm region. In addition, the 3.13 % standard also showed peaks close to 50 nm and 500 nm. Peaks below a relative frequency of 0.002 % were determined as noise. In summary, DLS seemed to mainly detect aggregation in AT standards as functions of the monomer peak. Indication of aggregation was detected in the standards with or above 0.78 % aggregates initially as a decrease of monomer peak intensity. Changes could also be seen as widening of the monomer peak at higher aggregate concentrations. The most prominent common aggregate size was 30 nm, visible in the 6.25 and 12.5 % standards. The 3.13 % standard also had a peak in this range, indicating the presence of this oligomer, possibly a penta- or hexamer if composed of intact, monomeric mAbs.
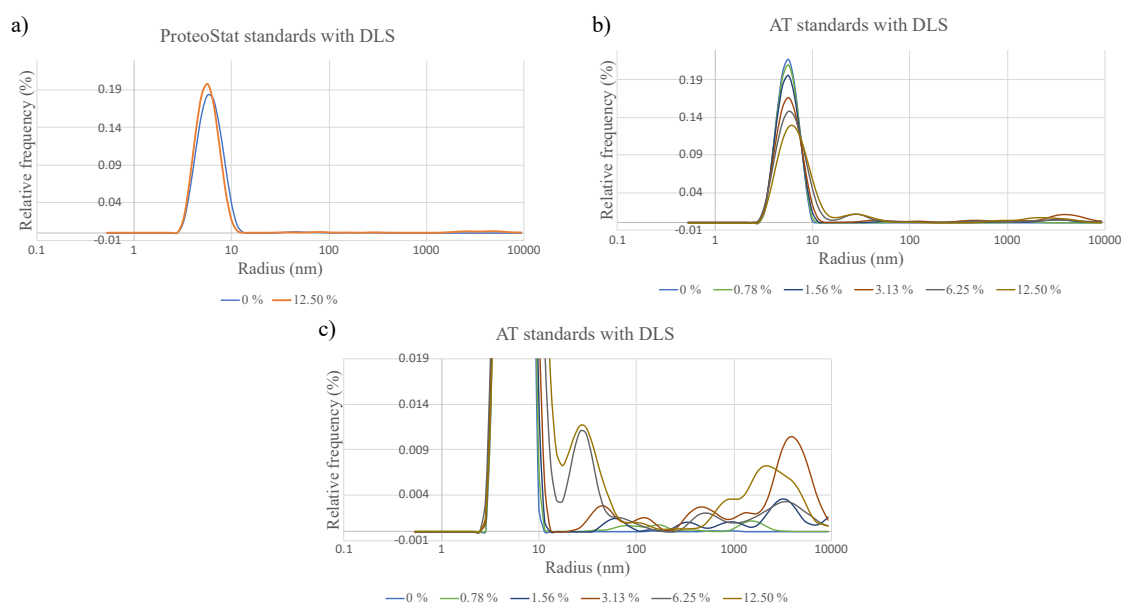
Figure 10. The a) ProteoStat and b), c) AT Aggregation-% standards analyzed with DLS.

Lastly, both sets of standards were analyzed with SEC-MALS. The chromatograms obtained for the ProteoStat and AT standards are shown in *Figures 11.* and *12*. The main peak in both ProteoStat and AT standards represented the monomeric mAb. The intensity of this monomer peak decreased to the increasing aggregate content similarly within both standard sets. With the ProteoStat standards, two higher molecular weight peaks were visible, while with the AT standards, only one slight hump preceding the monomer peak was detected. In addition, fragments were visible with the ProteoStat standards but not with the AT standards. Interestingly with the ProteoStat standards, even the 0 % standard containing solely monomer had the same content as the standard containing 12.5 % of aggregates. On the other hand, all the AT standards contained mainly the monomer peak. With both standard sets, the derived MWs for the main peaks were approximately 140 kDa (*Table 6.* and *7.*). These were slightly underestimated since 150 kDa is the general molecular weight of IgGs[55]. With the ProteoStat standards, the first peak preceding the monomer peak had an MW of approximately 273 kDa (*Table 6.*), indicating that it likely contained a dimer. The MWs determined for the first peaks eluted at around 5 min varied between the standards. The uneven MW curves indicated that the peaks were not homogeneous even within the individual standards. Based on the derived MWs, the peaks contained oligo- and/or multimers. Similarly, with the AT standards, the peak preceding the monomer peak had different MWs increasing with the aggregate concentration. The MW of peak 2 varied between 231–737 kDa (*Table 7.*).

For both standard sets, the r_H determined for the monomer peaks with flow mode DLS were underestimated compared to batch mode DLS (*Table 6.* and *7.*). Especially with the aggregate peaks, the r_H measurements suffered from very high uncertainties (%), which makes the derived values unreliable. The mass recoveries for the ProteoStat standards varied between almost 100 % and below 90 %, and for the AT standards, between 94 % and 78 %, as the aggregate concentration increased. The decrease was not linear with either standard set. This is also visible in *Figures 11.* and 12., where no changes except the monomer peak decrease are observed in relation to the increasing aggregate content. The recoveries of the AT standards were lower than the ProteoStat standards, with already around 7 % of sample loss with the 0 % standard. The low sample recoveries suggest that sample loss occurred. The sample pretreatment likely affected the recoveries, and larger aggregates never entered the system. With both standard sets, the mass fractions of the aggregates were not in accordance with the actual aggregate content of the samples but under- or over-estimated. In conclusion, SEC-MALS only detected the increasing aggregate contents of the standards as slight decreases in the monomer peak intensities.
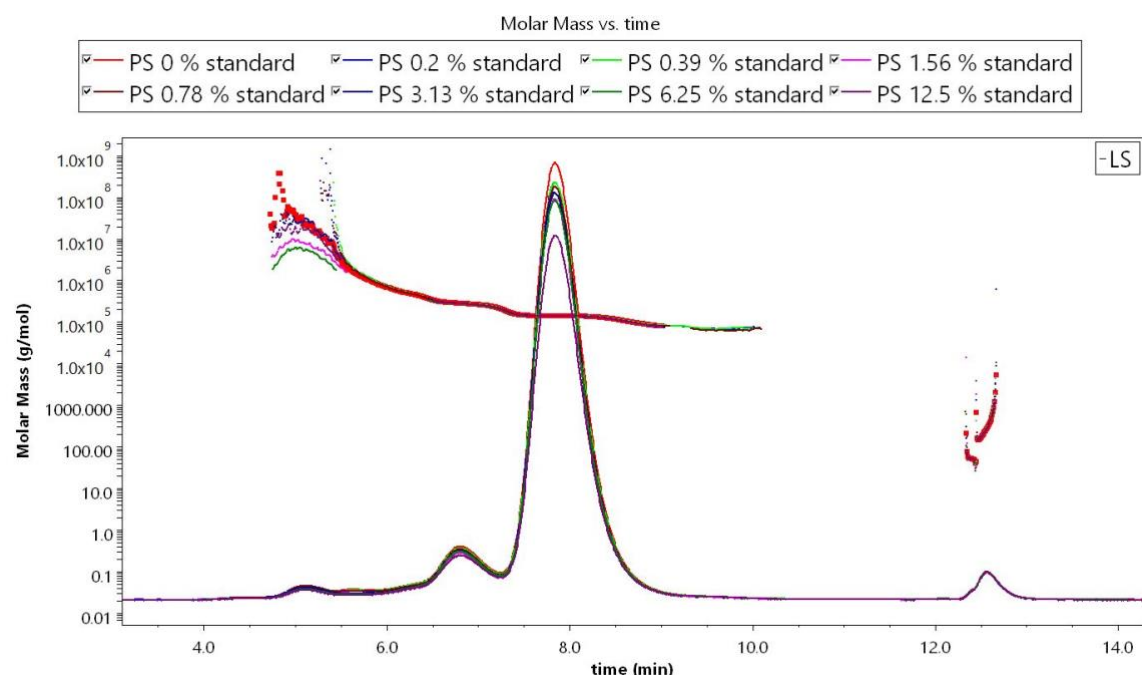

Figure 11. Chromatograms obtained with SEC-MALS of the ProteoStat Aggregation-% standards with the molar mass curves visible.

Table 6. Molecular weights and hydrodynamic radii determined for the first three peaks of the ProteoStat Aggregation-% standards analyzed with SEC-MALS.

| SEC-MALS data		Peak 1 7.2–9.0 min		Peak 2 6.5–7.2 min			Peak 3 4.7–6.5 min		
	Mass recovery (%)	Mw (kDa)	rn (nm)	Mw (kDa)	rn (nm)	Mass fraction (%)	Mw (kDa)	rn (nm)	Mass fraction (%)
PS 0% standard	98.3	138.6	4.1	276.5	7.7	0.6	976	12.9	0.1
PS 0.2% standard	93.2	138.7	5.3	275	8.1	0.7	715.1	13.4	0.1
PS 0.39% standard	94.1	138.5	5.4	277	7.1	0.7	699.7	10.6	0.1
PS 0.78% standard	93.0	138.1	5.1	275.6	7.5	0.7	741.1	11.9	0.1
PS 1.56% standard	89.9	138.0	5.1	269.2	9.6	0.6	5070.7	46.4	0
PS 3.13% standard	92.0	137.9	3.5	271.2	8.3	0.6	15181.6	46.8	0
PS 6.25% standard	91.0	138.2	4.5	268.6	7.7	0.6	4016.3	57	0
PS 12.5% standard	83.4	138.0	4.7	271.2	7.6	0.6	11352.6	46.4	0
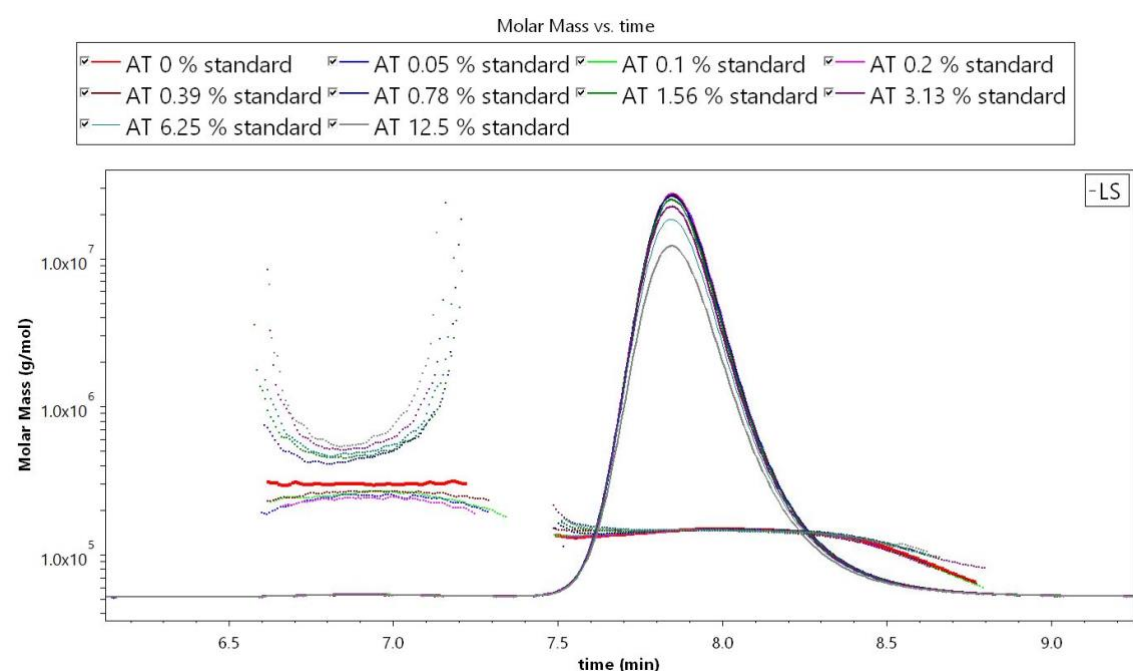
Figure 12. Chromatograms obtained with SEC-MALS of the AT Aggregation-% standards with the molar mass curves visible.

Table 7. Molecular weights and hydrodynamic radii determined for the two peaks of the AT Aggregation-% standards analyzed with SEC-MALS.

SEC-MALS data		Peak 1 7.5–8.7 min		Peak 2 6.6–7.3 min		
	Mass recovery (%)	Mw (kDa)	rn (nm)	Mw (kDa)	rn (nm)	Mass fraction (%)
AT 0 % standard	93.1	141.6	5	299.2	2.9	0.3
AT 0.05 % standard	93.8	141.9	4.8	236.2	12.9	0.5
AT 0.1 % standard	93.8	141.1	4.7	246.1		0.5
AT 0.2 % standard	93.8	141.8	4.2	231		0.4
AT 0.39 % standard	93.3	141.3	4.9	257.5	17.3	0.4
AT 0.78 % standard	89.9	144.1	5.1	517.6	15.1	0.2
AT 1.56 % standard	88.5	144	4.4	565.9	6.1	0.2
AT 3.13 % standard	86.6	143.8	3	660.5		0.1
AT 6.25 % standard	84	144.3	4.2	589.7	14.6	0.2
AT 12.5 % standard	77.6	144.6	4.4	736.9	14.4	0.1

The ProteoStat Aggregation-% standards are designed to be used with the ProteoStat probe to quantify aggregates in protein samples. Similar to the AT standards, ProteoStat standards are also made with native IgG spiked with different amounts of aggregated IgG. Despite this, especially the probes detected them slightly differently. The differences between the two standard sets could be caused by the fact that the AT standards were

produced by using very high heat, which most likely resulted in large aggregates. This is supported by the data obtained with DLS and SYPRO Orange, which had a 2-fold improvement in LLD with the AT standards. The probe has been previously reported to have a better sensitivity towards large aggregates[43]. It is also possible that the large aggregates dissociated into smaller units when highly diluted to create the lower standard concentrations. It is noteworthy that the Protein-Probe was sensitive enough to probe two different types of aggregates already from the ProteoStat standards, which could be caused by the high sensitivity of the probe towards larger aggregates. DLS and SEC-MALS shed light on the composition of the standards, and these methods also detected differences between the two standard sets. With SEC-MALS, the mass recoveries of both standard sets decreased when the aggregate amount changed from 0 % to 12.5 %. The ProteoStat standards consisted of small oligomers visible with SEC-MALS, while with the AT standards mainly the monomer peak was detected. This supports the idea that the AT standards consisted of larger aggregates that were likely lost in the centrifugation step before the analysis. Despite this, the main changes observed with both light scattering - methods were functions of the monomer peak.

3.3 Long-term incubation of trastuzumab and atezolizumab at elevated temperatures

The goal of this experiment was to obtain information about the aggregation process of the two studied mAbs and to determine how well the used analytical methods could detect small changes in the samples. Trastuzumab was incubated at 57 °C and atezolizumab at 53 °C for 11 days to obtain a slow and steady increase of aggregates. These temperatures were optimized to create a slow increase of aggregates in the samples over time. DLS was chosen as a reference method due to its extensive use in the industry, and the results were compared to the ones derived with ProteoStat and Protein-Probe. Trastuzumab and atezolizumab were chosen for this experiment based on their high concentrations.

The results of the DLS analysis for trastuzumab and atezolizumab are shown in *Figure 13*. For trastuzumab (*Figure 13a*)), the r_H of the monomer peak was approximately 5.7 nm with PDIs of 0.14, indicating a relatively homogeneous peak during the first 4 days. The monomer peak shifted towards larger particle sizes and widened with a simultaneous decrease in the peak intensity from day 7 of incubation forward. For atezolizumab, the intensity of the monomer peak decreased already from day 1 forward and started to shift simultaneously to larger particle sizes and widen (*Figure 13b*)). With trastuzumab, the

radius gradually increased with the PDI, and on day 11, the radius was 6.7 nm with a PDI of 0.53. The results were similar to the AT standards, but the changes were more modest. Similar to the AT standards, a peak at around 30 nm was visible for the day 11 sample. For atezolizumab, an r_H of 6 nm was obtained for the monomer peak of the native, unstressed sample. On day 3, the r_H was already 7.2 nm with a PDI of 0.56, and on day 11, the monomer peak shifted to 17 nm. On days 3 and 4, a slight hump appeared at around 20 nm for atezolizumab. From day 7 to 11, the shape of the former monomer peak morphed into a size distribution of dual peaks where the intensity of the monomer peak was significantly smaller than a new peak at around 20 nm. DLS could not separate the two peaks from each other, which was also observed in the r_H of the monomer peak. In conclusion, DLS started to detect changes in the trastuzumab sample from day 9 forward and the atezolizumab sample from day 1 forward.
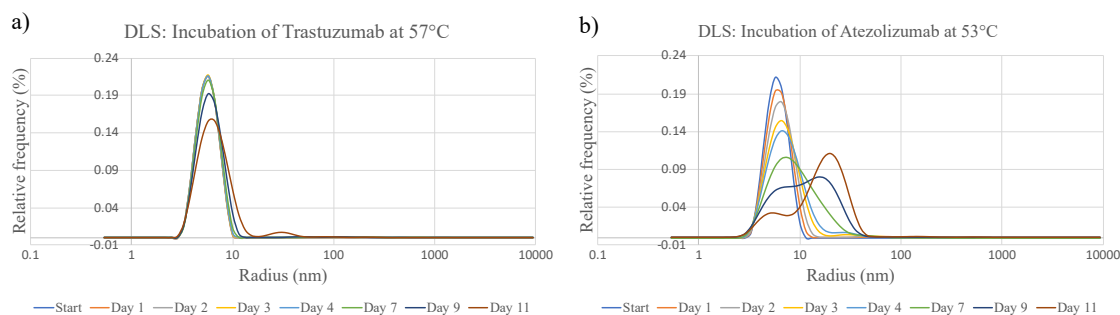

Figure 13. The size distributions of a) trastuzumab incubated at 57 °C and b) atezolizumab incubated at 53 °C produced with DLS.

The results obtained with ProteoStat and the Protein-Probe for trastuzumab and atezolizumab are presented in *Figure 14*. Neither of the probes detected any aggregation for trastuzumab during the first two days of incubation. On day 3, the signal started to deviate from the native mAb with both methods. With ProteoStat, the S/B-ratio increased from day 3 forward. On day 7, the S/B-ratio with ProteoStat was over 3, indicating that 7 days was the LLD for ProteoStat in this experiment. On day 7, the aggregation-% obtained with ProteoStat for trastuzumab was over 1 % (*Table 8.*). With the Protein-Probe, the S/B-ratio started to increase from day 4 forward. Despite the one-day delay in the increase of the S/B-ratio for the Protein-Probe, it also had an LLD of 7 days, at which point the aggregation-% was slightly over 0.1 % (*Table 8.*). On day 11, the Protein-Probe method had an S/B-ratio of 2x larger than ProteoStat. For atezolizumab, on day 1, the signal of ProteoStat had doubled, and it increased until day 2, which was the LLD. On day 2 with ProteoStat, the aggregation-% was approximately 2 % (*Table 9.*). After day 2, the signal was steady until day 9. This makes the LLD of 2 days for ProteoStat

questionable. For Protein-Probe, the S/B-ratio increased slightly every day. On day 7, the S/B-ratio exceeded 3, and the aggregation-% was approximately 0.3 % (*Table 9.*). Contrary to the trastuzumab samples, ProteoStat seemed to have higher S/B-ratios for atezolizumab than the Protein-Probe.
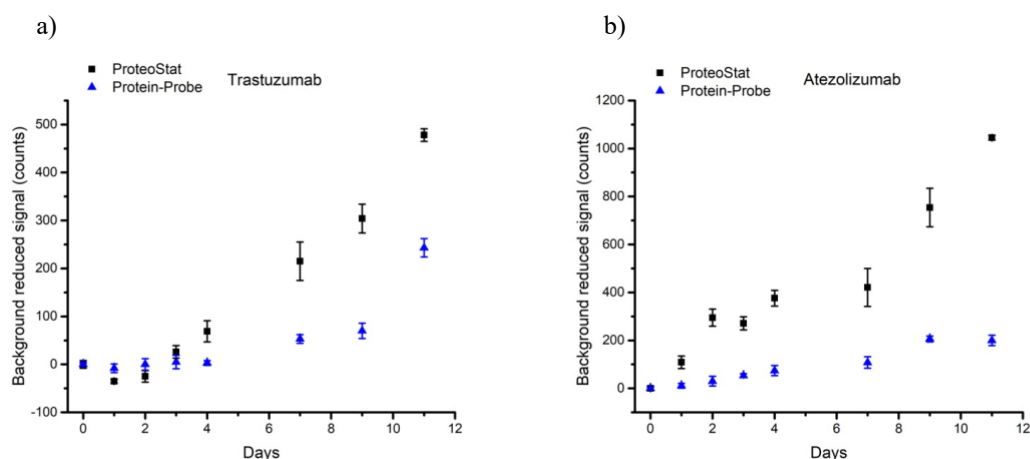

Figure 14. The background reduced signals for a) trastuzumab and b) atezolizumab during the 11-day incubation obtained with ProteoStat and Protein-Probe.

The two standard curves obtained with ProteoStat gave quite a similar aggregation-% for the samples, with more variation starting to occur with the higher aggregate content. Also, the two standard curves produced with Protein-Probe were in accordance with the aggregation-% evaluations. The Protein-Probe method evaluated the aggregation-% of the samples to significantly lower than ProteoStat. The aggregation-%s obtained with Protein-Probe were approximately 10x lower than with ProteoStat. The results obtained with the ProteoStat probe and the ProteoStat standards can be considered the most accurate, since they are designed to be used together.

Table 8. The aggregation-% of trastuzumab during the 11-day incubation obtained with ProteoStat and Protein-Probe using the two standard curves.

Aggregation-% of trastuzumab incubated at 57 °C				
	ProteoStat		Protein-Probe	
	PS standard curve	AT standard curve	PS standard curve	AT standard curve
LLD (Aggregation-%)	0.53	0.53	0.070	0.063
Day	Aggregation-% ± SD	Aggregation-% ± SD	Aggregation-% ± SD	Aggregation-% ± SD
0	0.41 ± 0.04	0.60 ± 0.07	0.026 ± 0.006	0.083 ± 0.020
1	0.26 ± 0.02	0.36 ± 0.04	0.014 ± 0.012	0.063 ± 0.071
2	0.30 ± 0.06	0.44 ± 0.09	0.025 ± 0.016	0.082 ± 0.065
3	0.52 ± 0.06	0.78 ± 0.11	0.033 ± 0.019	0.092 ± 0.065
4	0.70 ± 0.10	1.1 ± 0.2	0.030 ± 0.008	0.088 ± 0.026
7	1.3 ± 0.2	2.1 ± 0.3	0.12 ± 0.02	0.16 ± 0.03
9	1.7 ± 0.2	2.8 ± 0.3	0.15 ± 0.03	0.18 ± 0.04
11	2.4 ± 0.1	4.1 ± 0.2	0.55 ± 0.08	0.32 ± 0.04

Table 9. The aggregation-% of atezolizumab during the 11-day incubation obtained with ProteoStat and Protein-Probe using the two standard curves.

Aggregation-% of atezolizumab incubated at 53 °C				
	ProteoStat		Protein-Probe	
	PS standard curve	AT standard curve	PS standard curve	AT standard curve
LLD (Aggregation-%)	0.53	0.53	0.070	0.063
Day	Aggregation-% ± SD	Aggregation-% ± SD	Aggregation-% ± SD	Aggregation-% ± SD
0	0.54 ± 0.05	0.81 ± 0.08	0.066 ± 0.011	0.13 ± 0.02
1	1.0 ± 0.1	1.6 ± 0.2	0.086 ± 0.018	0.14 ± 0.03
2	1.8 ± 0.2	2.9 ± 0.3	0.14 ± 0.04	0.17 ± 0.05
3	1.7 ± 0.1	2.7 ± 0.3	0.17 ± 0.02	0.19 ± 0.02
4	2.1 ± 0.2	3.5 ± 0.3	0.21 ± 0.04	0.21 ± 0.05
7	2.3 ± 0.4	3.9 ± 0.7	0.31 ± 0.06	0.25 ± 0.05
9	3.6 ± 0.4	6.3 ± 0.7	0.52 ± 0.07	0.31 ± 0.03
11	4.8 ± 0.2	8.6 ± 0.5	0.50 ± 0.08	0.31 ± 0.04

This experiment shed light on the aggregation process of trastuzumab and atezolizumab. The DLS data of heat-stressed trastuzumab revealed that the AT standards contained large particles over 1 μm, while incubation at 57 °C led to a slow increase of smaller aggregates below 100 nm. A lag phase of more than 4 four days was observed with the probes, and changes were detected from day 7 forward. On the other hand, DLS started to detect aggregation from day 9 forward as a decrease of the monomer peak intensity. DLS data also revealed that the only clear aggregate had an r_H of approximately 30 nm. It is likely that the trastuzumab aggregates were reversible due to their small size and slow formation. The incubation of atezolizumab at 53 °C was also optimal in inducing a slow increase of aggregates. DLS and ProteoStat detected changes in the sample starting from day 1. The Protein-Probe was slower at detecting the aggregation. First, DLS detected changes regarding only the monomer peak, but from day 3 forward, small aggregates in the size of 20 nm, possibly tetramers, started to form. Upon longer incubation, the size distribution seemed to shift from a monomer to a small oligomer. On day 11, most of the monomer had disappeared, and the oligomer was the dominating species. According to ProteoStat and the ProteoStat standard curve, on day 11, atezolizumab had aggregation of approximately 5 % and trastuzumab 2 %.

3.4 Short-term incubation of mAbs at elevated temperatures

The purpose of this experiment was to obtain more aggregation faster than in the long-term incubation, and this was done by incubating all the studied mAbs at higher temperatures of 60 °C and 70 °C. The goal was to achieve still sub-visible aggregates, which has been previously done by incubating antibodies at 70 °C for 10 min[56].

Incubation at 60 °C for 10 min was chosen as an additional condition to assess the sensitivity of the studied methods.

The results obtained with the probes are presented in *Graph 1.* and *Table 10. as* S/B-ratios and aggregation-%s. With the Protein-Probe method, an abnormally high signal was obtained for the detection solution, which may be reflected in the results. For ProteoStat, SYPRO Orange, and Protein-Probe, the CV % varied between 2–41 %, 3–28 %, and 4–71 %, respectively. The S/B-ratios at 60 °C were mainly below 2, which means that only minimal aggregation was detected compared to the native mAb. This was also seen in the aggregation-%s. Of all the mAbs, only bococizumab had S/B-ratio at 60 °C, indicative of substantial aggregation with all the probes. This was expected since the mAb had a T_m-value below 60 °C. Generally, the incubation at 70 °C caused a significant signal increase for all mAbs detected by the probes, except for trastuzumab. Trastuzumab excluded, the S/B-ratios obtained for the other mAbs at 70 °C with ProteoStat, SYPRO Orange and Protein-Probe varied between 11–26, 5.6–19 and 5.5–77, respectively. The aggregation-% for these samples mainly varied between 3.3 and 21 %, depending on the probe and the standard curve used. The Protein-Probe had the most variation in the S/B-ratios, which shows that the probe binds the aggregates with the most specific interactions.

Only one standard sample was used for SYPRO Orange to equalize the signals to the ProteoStat standard curve. The amounts of aggregates detected were relatively uniform between ProteoStat and SYPRO Orange. With Protein-Probe, the estimated aggregation-%s for the samples were again significantly lower with the lowest estimates obtained with the AT standard curve. The Protein-Probe estimated the aggregation-% of atezolizumab incubated at 70 °C to be similar to the other probes when the ProteoStat standard curve was used. For the same sample, Protein-Probe had an S/B-ratio of 77. This shows that the used standards are not optimal to be used with the Protein-Probe. In addition, all probes detected small amounts of aggregation already in the native samples.
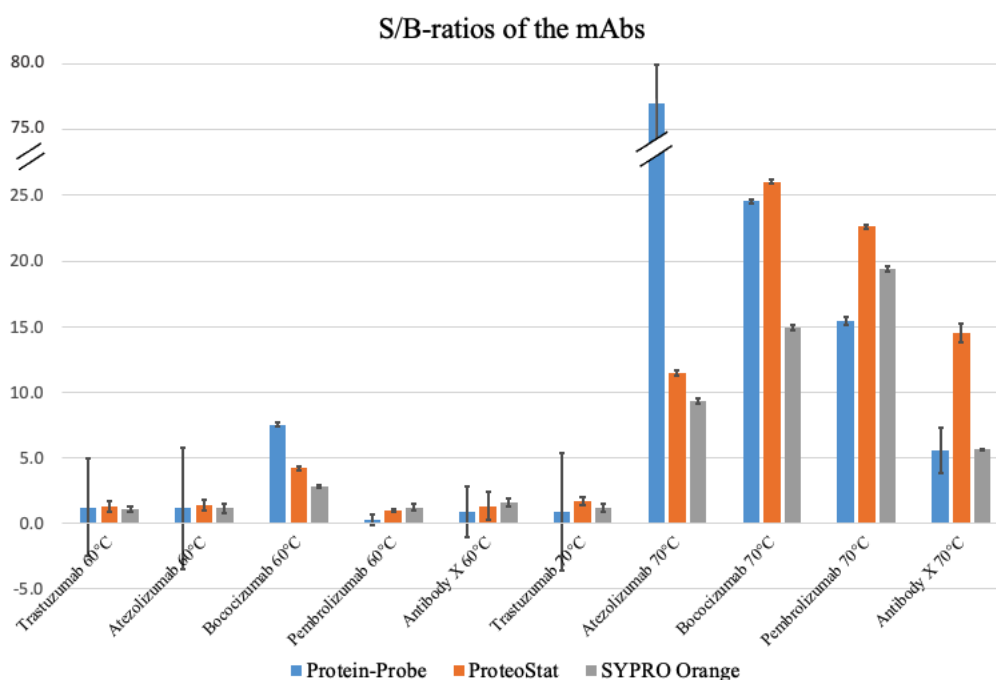
Graph 1. The S/B-ratios of all the mAbs incubated at 60 °C and 70 °C for 10 min. The used background was the signal of the native, unstressed mAb. The SDs are presented as black lines.

Table 10. The aggregation-% of the mAbs incubated at 60 °C and 70 °C for 10 min according to the probes with both standard curves.

Aggregation-% of mAbs incubated in 60 °C and 70 °C for 10 minutes						
	ProteoStat		SYPRO Orange		Protein-Probe	
	PS standard curve	AT standard curve	PS standard curve	AT standard curve	PS standard curve	AT standard curve
LLD (Aggregation-%)	0.53	0.53	0.57	0.21	0.070	0.063
	Aggregation-% ± SD	Aggregation-% ± SD	Aggregation-% ± SD	Aggregation-% ± SD	Aggregation-% ± SD	Aggregation-% ± SD
Trastuzumab native	0.40 ± 0.08	0.63 ± 0.13	0.58 ± 0.07	0.59 ± 0.09	0.018 ± 0.013	0.084 ± 0.055
Trastuzumab 60°C	0.50 ± 0.16	0.80 ± 0.27	0.60 ± 0.02	0.61 ± 0.03	0.022 ± 0.013	0.091 ± 0.048
Trastuzumab 70°C	0.66 ± 0.13	1.1 ± 0.2	0.68 ± 0.07	0.70 ± 0.10	0.015 ± 0.014	0.077 ± 0.066
Atezolizumab native	0.47 ± 0.11	0.76 ± 0.18	0.63 ± 0.07	0.65 ± 0.10	0.019 ± 0.015	0.086 ± 0.063
Atezolizumab 60°C	0.53 ± 0.17	0.86 ± 0.29	0.70 ± 0.12	0.72 ± 0.16	0.023 ± 0.022	0.091 ± 0.078
Atezolizumab 70°C	4.9 ± 0.37	9.5 ± 0.8	5.5 ± 0.3	6.1 ± 0.5	3.5 ± 0.5	0.85 ± 0.09
Bococizumab native	0.44 ± 0.06	0.70 ± 0.09	0.82 ± 0.08	0.86 ± 0.11	0.01 ± 0.02	0.17 ± 0.03
Bococizumab 60°C	1.7 ± 0.20	3.1 ± 0.4	2.2 ± 0.1	2.4 ± 0.1	1.1 ± 0.1	0.50 ± 0.04
Bococizumab 70°C	10 ± 1	21 ± 2	11 ± 1	13 ± 2	4.4 ± 0.6	0.94 ± 0.09
Pembrolizumab native	0.50 ± 0.07	0.81 ± 0.12	0.63 ± 0.05	0.65 ± 0.07	0.12 ± 0.04	0.19 ± 0.05
Pembrolizumab 60°C	0.49 ± 0.03	0.79 ± 0.05	0.75 ± 0.10	0.77 ± 0.14	0.024 ± 0.009	0.095 ± 0.031
Pembrolizumab 70°C	10 ± 1	21 ± 2	11 ± 1	13 ± 2	3.3 ± 0.5	0.83 ± 0.08
Antibody X native	0.25 ± 0.09	0.38 ± 0.15	0.90 ± 0.04	0.94 ± 0.06	0.026 ± 0.015	0.10 ± 0.05
Antibody X 60°C	0.32 ± 0.13	0.49 ± 0.21	1.4 ± 0.3	1.5 ± 0.5	0.022 ± 0.007	0.091 ± 0.027
Antibody X 70°C	3.3 ± 0.3	6.1 ± 0.5	4.8 ± 0.2	5.4 ± 0.3	0.19 ± 0.03	0.24 ± 0.03

The size distributions obtained with DLS are shown in *Figure 15*. Trastuzumab was the only mAb that showed essentially no difference in the size distributions between the native and stressed samples. The size distribution between the native mAb and the mAb incubated at 60 °C was similar with atezolizumab and antibody X. With pembrolizumab, the intensity of the monomer peak in the 60 °C sample had slightly decreased, and with bococizumab, the monomer peak had additionally shifted to larger particle sizes. The incubation at 70 °C had shifted the monomer peak to a larger particle size of approximately 20 nm and decreased its intensity for all mAbs except trastuzumab. With atezolizumab, the sample incubated at 70 °C also showed a shoulder at the particle size

of the monomeric mAb. No other particles than the monomer peak were visible in the samples.
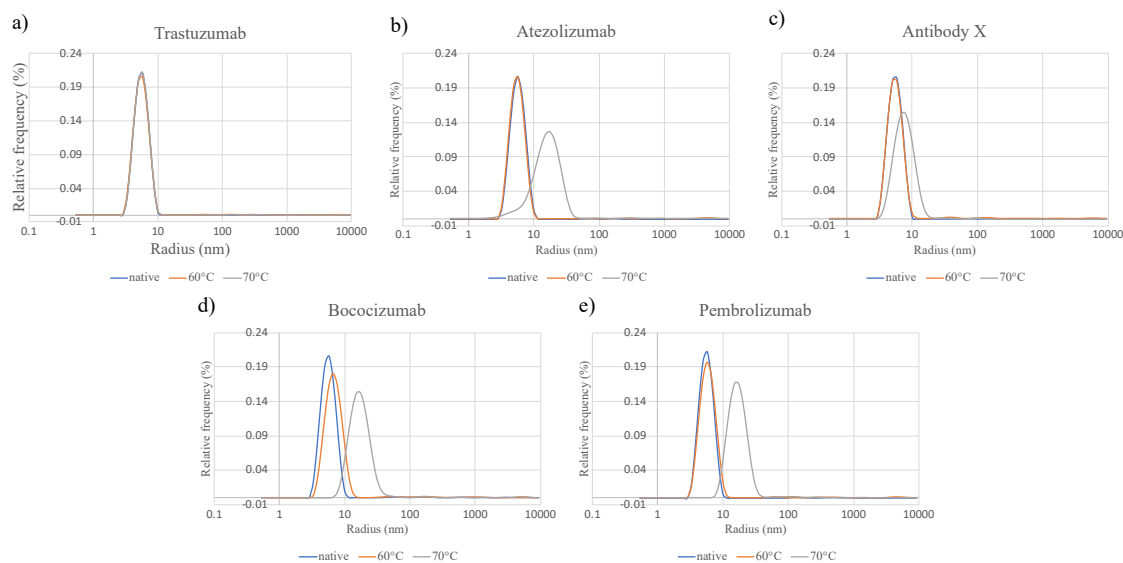

Figure 15. The size distributions obtained with DLS of a) trastuzumab, b) atezolizumab, c) antibody X, d) bococizumab and e) pembrolizumab unstressed and after incubation at 60 °C and 70 °C.

Two sets of these samples were prepared for SEC-MALS because the first analysis did not give any peaks for the bococizumab and pembrolizumab samples. In the second attempt, all the samples had aggregate peaks at the same retention times, even the native ones. This indicated that aggregation could have occurred in the column due to, for example, absorption of a sticky aggregate, which could have induced aggregation in the other samples. Also, the elution times did not, in all cases, follow the decreasing size, indicating secondary interactions between the column and the samples. It was deduced that the information from the second attempt did not reflect the actual sample compositions. Hence, the data from the first SEC-MALS analysis is presented here. As a result, no SEC-MALS data is given for the bococizumab and pembrolizumab samples.

The data obtained for trastuzumab, atezolizumab, and antibody X by SEC-MALS are shown in *Figures 16., 17.* and *18.* as chromatograms with the MW curves visible. Also, the MWs of the relevant peaks, the hydrodynamic radii, mass fractions, and mass recoveries of all the three mAbs are presented in *Table 11*. In the chromatograms mainly monomer peaks were visible for the samples, and only a small amount of higher molecular weight components were detected. The monomer peak intensities decreased but were not fully in accordance with the amount of stress induced. The MWs of the main peaks all corresponded to that of a monomer, with slight undervaluations. The small humps preceding the monomer peaks had different MWs between the samples with mostly

negligible mass fractions, which were not in accordance with the probes. However, the mass fraction obtained for the hump of antibody X incubated at 70 °C was the same magnitude as ProteoStat and SYPRO Orange estimated the aggregation-%. The MWs of the preceding peaks suggested the presence of aggregates, but their composition was hard to reason. Most likely, the monomers present in the aggregates had conformationally altered structures. Also, their content was not homogeneous, and the uncertainties (%) for these MW estimates were high. Additionally, SEC-MALS had trouble estimating the r_H for the components. The mass recoveries of the samples varied greatly, with the worst obtained for atezolizumab samples. Atezolizumab incubated at 70 °C had only a 36 % sample recovery.
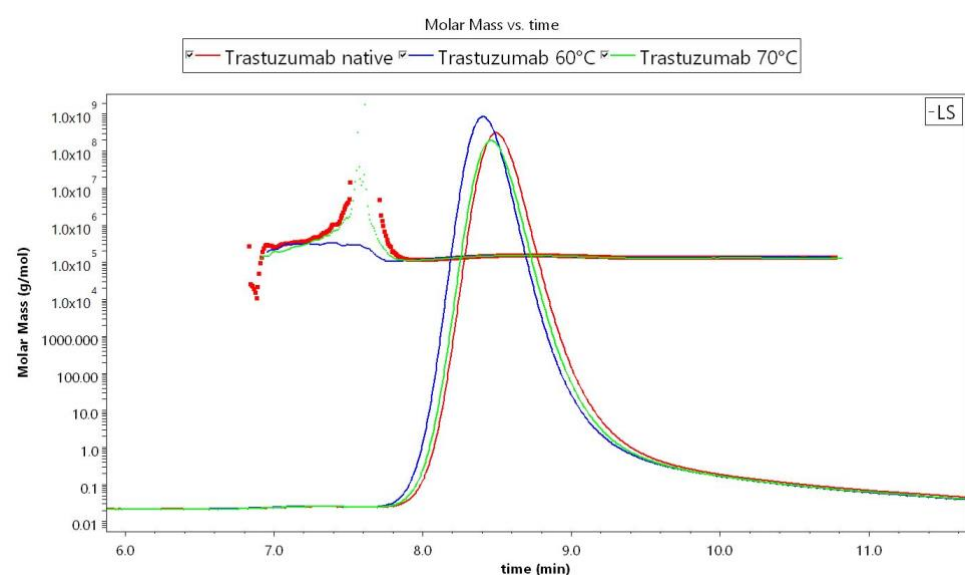

Figure 16. Chromatograms of the trastuzumab samples incubated at 60°C and 70°C obtained with SEC-MALS with the MW curves visible.
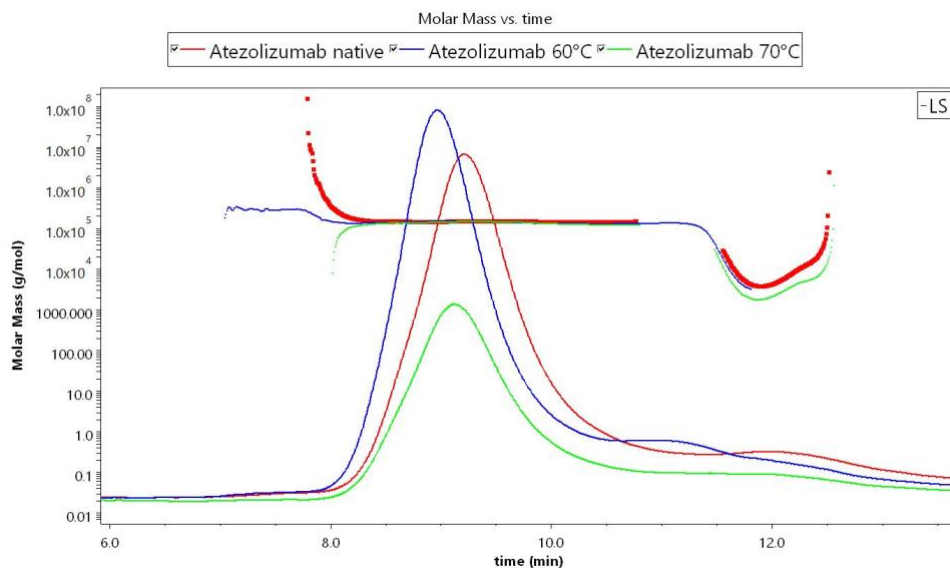
Figure 17. Chromatograms of the atezolizumab samples incubated at 60 °C and 70 °C obtained with SEC-MALS with the MW curves visible.
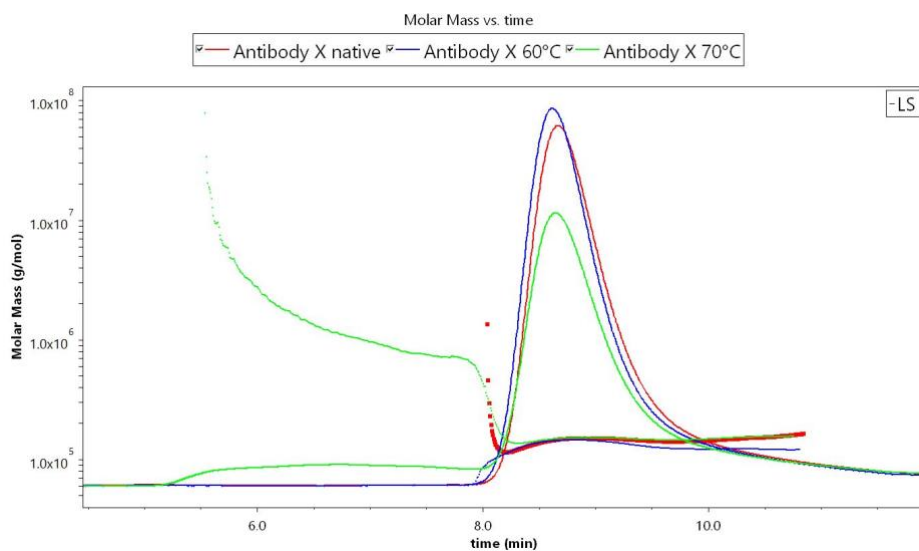

Figure 18. Chromatograms of the antibody X samples incubated at 60 °C and 70 °C obtained with SEC-MALS with the MW curves visible.

Table 11. Relative information obtained with SEC-MALS of trastuzumab, atezolizumab and antibody X incubated at 60 °C and 70 °C.

SEC-MALS data		Peak 1 (7.8–10.8 min)		Peak 2 (6.9–7.8 min)		
	Mass recovery (%)	Mw (kDa)	rn (nm)	Mw (kDa)	rn (nm)	Mass fraction (%)
Trastuzumab native	85.2	140.3	5.2	501.8	45.3	0.1
Trastuzumab 60°C	86.2	141.1	4.2	254.6		0.2
Trastuzumab 70°C	83.5	139.4	4.3	356		0.1
		Peak 1 (7.9–10.7 min)		Peak 2 (7.0–7.9 min)		
	Mass recovery (%)	Mw (kDa)	rn (nm)	Mw (kDa)	rn (nm)	Mass fraction (%)
Atezolizumab native	60.3	146.5	4.2	1376		0
Atezolizumab 60°C	66.2	142.1	4.1	265.9		0.2
Atezolizumab 70°C	35.8	138.2				0
		Peak 1 (8.0–10.8 min)		Peak 2 (5.2–8.0 min)		
	Mass recovery (%)	Mw (kDa)	rn (nm)	Mw (kDa)	rn (nm)	Mass fraction (%)
Antibody X native	79.2	143.2	1.4			
Antibody X 60°C	88.4	135.3	2.6			
Antibody X 70°C	64.2	148.5	7.6	1107.6	13.9	1.3

SEC-MALS did not provide much information on the sample compositions, as it mainly indicated aggregation as functions of the monomer peaks. Also, SEC-MALS suffered from significantly low sample recoveries, and peak shapes indicated that the system would have benefited from optimization for these samples. The DLS data revealed that aggregates below 50 nm in r_H were present in the samples incubated at 70 °C, but due to poor resolution, the peaks also contained the monomeric mAb. The probes were in accordance with the DLS data, and the most aggregated samples were bococizumab and pembrolizumab incubated at 70 °C. ProteoStat and SYPRO Orange evaluated these samples to have aggregation at around 10 %. While significant aggregation could be expected for bococizumab, for pembrolizumab, it was surprising since the mAb had a very similar T_m to atezolizumab and antibody X.
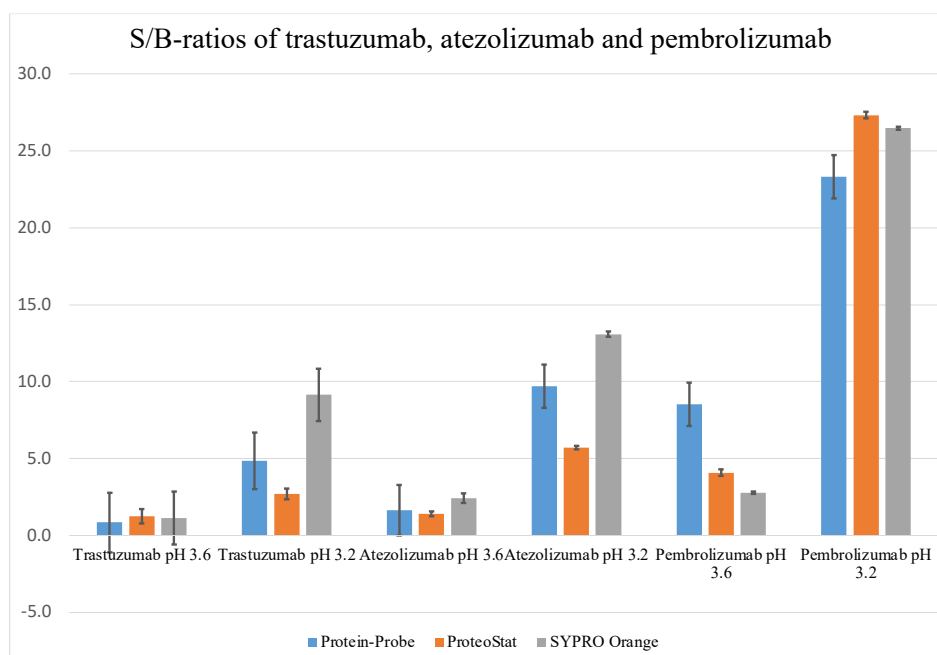
3.5 Low pH incubation of trastuzumab, atezolizumab and pembrolizumab

Aggregation was induced on three mAb samples by incubation at low pH and then returning the pH near neutral. The goal of this experiment was to see the effect of low pH on aggregation, and it was designed to mimic the viral inactivation process that occurs in mAb production. In the viral inactivation process, the pH is kept at 3.6 for several hours to inactivate any viruses and then returned to a near-neutral pH[57]. To ensure the formation of aggregates, an additional pH of 3.2 was used, and both low pH incubations were carried out at 37 °C. Trastuzumab, atezolizumab, and pembrolizumab were chosen for this experiment based on their high concentrations. The results from the low pH incubation with the probes are shown in *Graph 2.* as S/B-ratios and in *Table 12.* as obtained aggregation-%s. For ProteoStat, SYPRO Orange, and Protein-Probe, the CV % varied between 5.3–35 %, 0.1–44 %, and 5.3–57 %, respectively.

The S/B-ratios obtained for the samples incubated at pH 3.6 were much lower than for those incubated at pH 3.2. None of the probes detected aggregation for trastuzumab incubated at pH 3.6, but for atezolizumab at pH 3.6, the S/B-ratios were over 1, with SYPRO Orange having the largest ratio of 2.4. For pembrolizumab at pH 3.6, the Protein-Probe had the highest S/B-ratio of 8.5, approximately 2–3x higher than ProteoStat and SYPRO Orange. As for the incubations conducted at pH 3.2, surprisingly, SYPRO Orange had the highest S/B-ratios for trastuzumab and atezolizumab. For pembrolizumab, the S/B-ratios were at the same level between the probes.

Only one standard sample was used for equalizing the sample signals to the trastuzumab standard curve for all the probes. The amount of aggregates present in the samples

followed the trend of the S/B-ratios. Trastuzumab incubated at pH 3.2 had approximately 1–2 % of aggregation, while atezolizumab and pembrolizumab had 5–20 %, depending on the used probe and standard curve. ProteoStat and SYPRO Orange gave relatively similar estimates for the aggregation-% for the samples. On the other hand, the Protein-Probe estimated them to be significantly lower again.

Graph 2. The S/B-ratios obtained with ProteoStat, SYPRO Orange, and Protein-Probe of trastuzumab, atezolizumab, and pembrolizumab incubated at pH 3.6 and pH 3.2. The used backgrounds are the signals received for the native, unstressed mAbs. Standard error bars are included as black lines.

Table 12. The aggregation-% of trastuzumab, atezolizumab, and pembrolizumab incubated at pH 3.2 and pH 3.6 according to the probes by using the ProteoStat and AT standard curves.

Aggregation-% of trastuzumab, atezolizumab and pembrolizumab incubated at pH 3.2 and pH 3.6						
	ProteoStat		SYPRO Orange		Protein-Probe	
	PS standard curve	AT standard curve	PS standard curve	AT standard curve	PS standard curve	AT standard curve
LLD (Aggregation-%)	0.53	0.53	0.57	0.21	0.070	0.063
	Aggregation-% ± SD	Aggregation-% ± SD	Aggregation-% ± SD	Aggregation-% ± SD	Aggregation-% ± SD	Aggregation-% ± SD
Trastuzumab pH 3.6	0.59 ± 0.19	0.83 ± 0.32	0.27 ± 0.03	0.33 ± 0.04	0.10 ± 0.10	0.010 ± 0.031
Trastuzumab pH 3.2	1.2 ± 0.1	1.9 ± 0.2	2.1 ± 0.2	2.7 ± 0.3	0.24 ± 0.05	0.25 ± 0.04
Atezolizumab pH 3.6	1.1 ± 0.2	1.6 ± 0.3	1.6 ± 0.3	2.1 ± 0.4	0.069 ± 0.024	0.14 ± 0.05
Atezolizumab pH 3.2	4.1 ± 0.3	6.7 ± 0.6	8.1 ± 0.5	11 ± 1	0.58 ± 0.09	0.36 ± 0.04
Pembrolizumab pH 3.6	2.6 ± 0.3	4.0 ± 0.6	2.8 ± 0.2	3.8 ± 0.4	0.48 ± 0.07	0.33 ± 0.04
Pembrolizumab pH 3.2	16 ± 2	29 ± 4	26 ± 1	37 ± 1	1.6 ± 0.2	0.56 ± 0.05

The results obtained with DLS of the samples are shown in *Figure 19*. The lower the pH, the more the monomer peaks decreased in intensity, shifted to larger particle sizes, and widened. Least changes were seen with trastuzumab and the most with pembrolizumab, which was in good accordance with the data obtained from the probes. Even though no significant changes could be seen for trastuzumab, the r_H of the main peak increased to over 6 nm after incubation at pH 3.6. However, the only deviating r_H of the main peak

occurred when pembrolizumab was incubated at pH 3.2. In these conditions, the r_H was 12 with a PDI of 0.53.
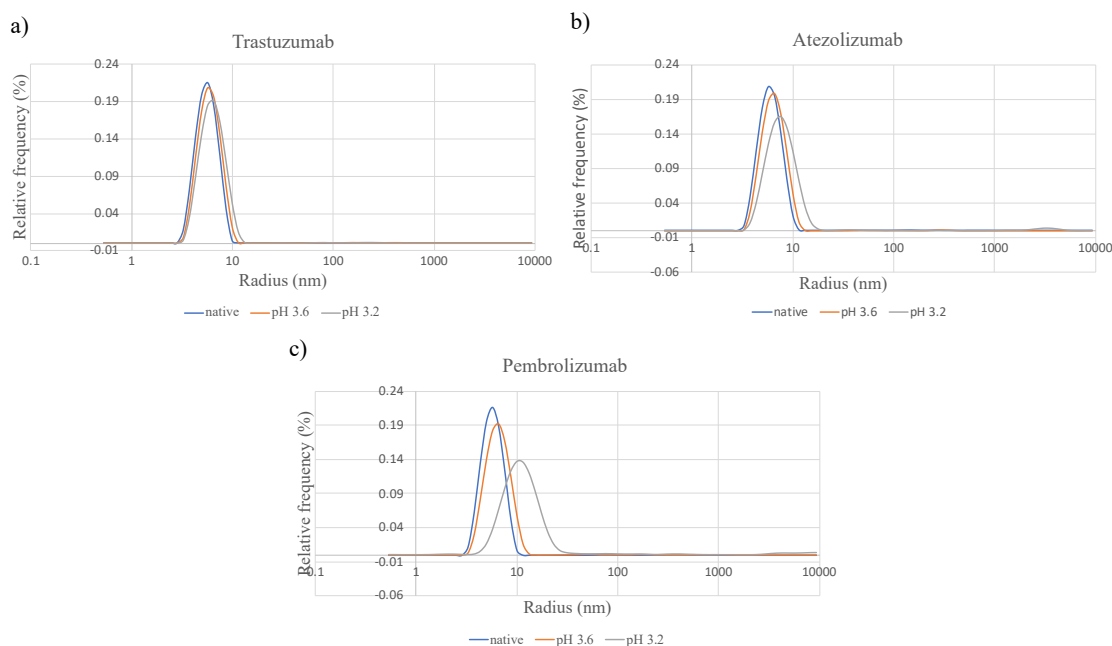

Figure 19. The size distributions obtained with DLS for a) trastuzumab, b) atezolizumab, and c) pembrolizumab unstressed and after incubation at pH 3.6 and pH 3.2.

The chromatograms with MW curves visible obtained with SEC-MALS for all the samples are presented in *Figures 20*., *21*. and *22*. In *Table 13*. are collected the obtained MWs and the hydrodynamic radii of the two first peaks, mass fractions of the higher MW peaks, and the mass recoveries for the whole samples. The decreasing monomer peak intensity was common for all the mAbs upon decreasing pH. In addition, all the mAb samples had a higher MW peak preceding the monomer peak except the native trastuzumab sample. The samples subjected to low pH also showed fragments eluting at later times.

For all the samples, the MWs of the monomer peaks corresponded to that of a monomeric IgG, though slightly underestimated. Pembrolizumab incubated at pH 3.6 made an exception since the MW of the monomer peak was 170 kDa. The PDI of this peak was also higher than the PDIs of the other monomer peaks. For trastuzumab and atezolizumab, the monomer preceding peaks of the stressed samples had MWs indicative of a dimer. For native pembrolizumab and pembrolizumab incubated at pH 3.2, the monomer preceding peaks had an MW similar to the monomer peak. This suggests that these are monomers with altered conformations. It is unclear why the unstressed sample also showed a presence of the altered structure, but it could be characteristic of the specific

44

mAb. This could explain why pembrolizumab was the least stable under this experimental setup. The mass fractions determined for the higher MW peaks corresponded with the aggregation-% obtained with the probes. For example, SEC-MALS determined the mass fraction of the aggregate in trastuzumab pH 3.6 –sample to be 0.4 %, while ProteoStat determined the aggregation-% to be 0.6 %. However, the mass fractions derived from SEC-MALS are not as trustworthy since significant sample loss occurred again. Upon incubation at low pH, the sample recoveries significantly decreased. The instrument was also unable to determine the hydrodynamic radii with the flow mode DLS for most of the peaks, and the ones obtained did not correlate with the MWs.
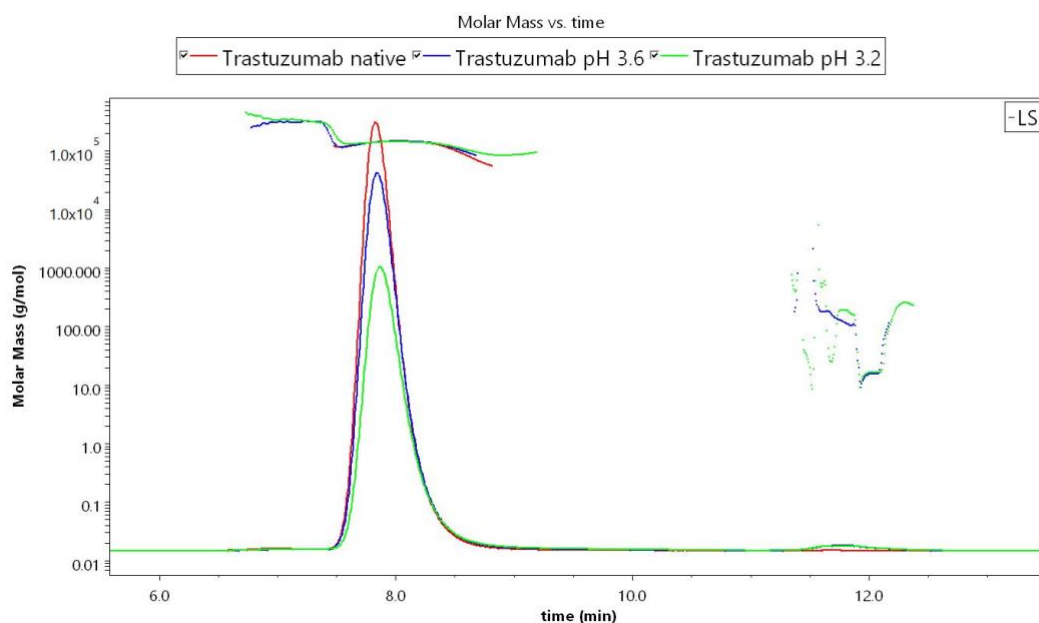

Figure 20. Chromatograms of trastuzumab samples before and after incubation at pH 3.6 and pH 3.2 obtained with SEC-MALS with the MW curves visible.
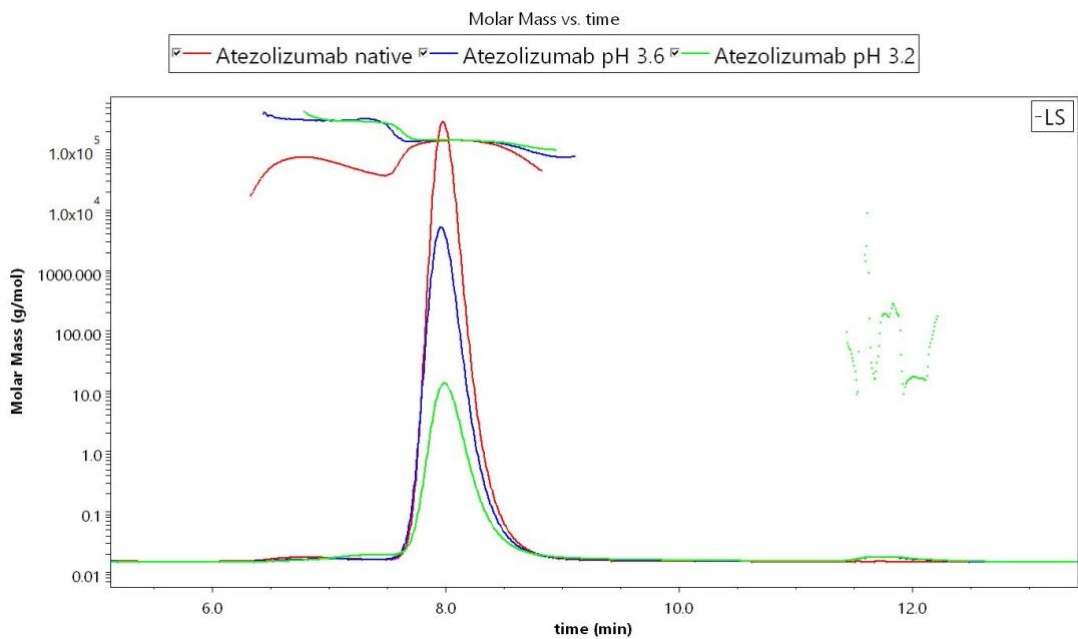
Figure 21. Chromatograms of atezolizumab samples before and after incubation at pH 3.6 and pH 3.2 obtained with SEC-MALS with the MW curves visible.
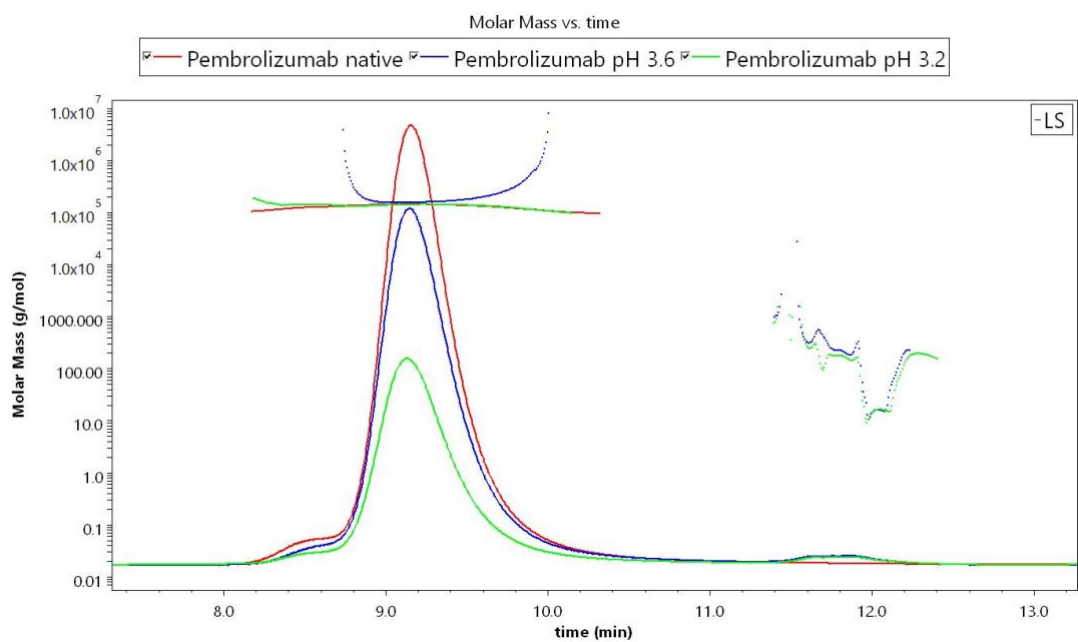

Figure 22. Chromatograms of pembrolizumab samples before and after incubation at pH 3.6 and pH 3.2 obtained with SEC-MALS with the MW curves visible.

Table 13. Relative information obtained from the analysis of the low pH -samples with SEC-MALS.

SEC-MALS data		Peak 1 (7.5–8.9 min)		Peak 2 (6.8–7.5 min)		
	Mass recovery (%)	Mw (kDa)	rn (nm)	Mw (kDa)	rn (nm)	Mass fraction (%)
Trastuzumab native	91.5	138.4				
Trastuzumab pH 3.6	84.4	139.3		241.1	7.3	0.4
Trastuzumab pH 3.2	66.1	138.2		339.8		0.3
		Peak 1 (7.6–9.0 min)		Peak 2 (6.5–7.6 min)		
	Mass recovery (%)	Mw (kDa)	rn (nm)	Mw (kDa)	rn (nm)	Mass fraction (%)
Atezolizumab native	105	132		55	10.7	4.5
Atezolizumab pH 3.6	73.2	139.7		311.7	6	0.7
Atezolizumab pH 3.2	42.5	141.7		292	7.2	2.3
		Peak 1 (8.7–10.2 min)		Peak 2 (8.2–8.7 min)		
	Mass recovery (%)	Mw (kDa)	rn (nm)	Mw (kDa)	rn (nm)	Mass fraction (%)
Pembrolizumab native	93.8	139.2		123.1		3.8
Pembrolizumab pH 3.6	48.1	172.8				
Pembrolizumab pH 3.2	46.3	139		143.6	5.8	2.8

All the methods were in accordance with each other, despite that SEC-MALS did not provide much information about the samples again. However, it did estimate the aggregation of trastuzumab to be more significant than DLS and the probes if the mass recoveries are regarded. Pembrolizumab seemed to be the most susceptible to aggregation induced by pH variation. The obtained T_m-values do not explain the higher aggregation of pembrolizumab since atezolizumab had a similar T_m-value to pembrolizumab.

4   Conclusions

NanoDSF produced reliably unfolding curves for all the mAbs, and the utilization of intrinsic luminescence is a clear benefit since it simplifies the experiments. The sensitivity of the method was similar to SYPRO Orange. However, the dynamic concentration range provided by the instrument manufacturer is extensive, which allows the analysis of mAbs at concentrations that are relevant in formulations. This specific instrument is then beneficial from mAb development to formulation studies. The performance of the method suffered from the presence of Triton X-100, and so it is not compatible with all excipients. However, this was also observed with ANS and SYPRO Orange. A clear disadvantage of nanoDSF is that it relies on the amount of luminescent amino acids present in the mAb structure, which can vary greatly and affect the mAb visibilities. The thermal unfolding curves generated with the external probes had more variance between different mAbs than what was observed with the curves produced with nanoDSF. In some cases, strong interactions with mAbs occurred at RT, which lowered the S/B-ratios and affected the mAb visibilities. Even if a clear transition is obtained with this kind of mAb-probe combination, the possible interferences to the unfolding event must be considered. However, it is possible that method optimization could have fixed the problems observed

with the probes. A much higher sensitivity was obtained with the FRET-probe than with nanoDSF, enabling very low sample consumption.

SYPRO Orange generally had a low luminescence signal at RT with the mAbs, which is desired from a luminescent probe used to probe differences between the native and altered structures. The probe's functionality also shows in the S/B-ratios of the unfolding curves. It functioned the most consistent among all the tested probes and was the most applicable for all the mAbs. This highlights its popularity in DSF measurements and reveals that it does not have highly specific interactions with the mAbs. Overall, a lack of specificity might be desired when analyzing a variety of mAb structures, and for that purpose, a hydrophobic probe seems to suit the best.

ANS performed the least optimal out of all the tested probes. The poor performance of ANS could be due to the use of surfactant[15] even at the lower concentration. ANS could have required a surfactant free assay to exhibit its full potential, but if so, it is a significant limitation e.g., in formulation studies. In addition, the dye needs to be excited in the UV region and hence is not as versatile as the other probes.

The FRET-probe exhibited varying results. It could be proposed that the peptide responsible for probing conformational changes is suboptimal for mAb structures like bococizumab, where the microenvironment of luminescent residues is polar already in the native conformation. It seems that the probe has an affinity towards some of the antibody structures at RT, and this causes it to lose its sensitivity towards the structural changes in the used conditions. For trastuzumab and pembrolizumab it worked exceptionally well, and for these mAbs, the F350/330 nm was low at RT, and so was the signal with FRET-probe. Thus, it can be reasoned that the mAb structure plays a crucial role in the ability of the probe to probe the conformational changes and subsequently provide good thermal unfolding curves.

All the methods produced thermal unfolding curves for all the mAbs. Out of the mAbs, trastuzumab exhibited the highest unfolding event at around 80°C and bococizumab the lowest at around 60°C. Bococizumab seemed to create the most deviating unfolding curves out of the mAbs. Not only did it cause a decreasing curve with the nanoDSF, but it also caused relatively high starting luminescence with all the external probes, especially with the FRET-probe and ANS. The decreasing 350/330 nm ratio for bococizumab at RT suggests that the luminescent amino acid residues are exposed to a polar environment instead of usually being buried in the structure. With nanoDSF, the assay window was

also reduced with bococizumab compared to the other mAbs. It can be deduced that the structure of bococizumab differs significantly from the other studied mAbs. It is also possible that the mAb sample was not entirely monomeric.

DLS was supposed to provide size distributions and hydrodynamic radii for the aggregated samples. Its main advantage is the non-destructiveness of the method reflecting the actual sample composition. It is also optimal for discovering even trace amounts of aggregates. The main phenomenon observed with DLS upon analyzing stressed samples was changes in the monomer peaks. The more aggregated the sample, the more the monomer peak decreased in intensity, widened, and shifted to larger particle sizes. Also, the PDI values increased simultaneously and indicated that DLS lacked the resolution to separate the components. In a few experiments, like atezolizumab incubated at 53 °C, DLS was able to show separation between the monomer peak and an aggregate peak at around 20 nm. One explanation for the changes in resolution is the working concentration ranges for specific particle sizes[34]. This could also explain why the instrument mostly only detected the monomer peak. In general, it can be deduced that the aggregation experiments caused mainly aggregates sized < 100 nm. As for particle sizes above 100 nm, only the AT standards seemed to contain large aggregates of even > 1 µm. However, the instrument could not determine exact particle sizes for most of the aggregate peaks. Usually, the r_H of aggregate peaks suffered from a SD of several hundred.

SEC-MALS is a standard method used to obtain qualitative and quantitative information about aggregated samples. Despite this, the high-pressure SEC-MALS suffered from serious drawbacks in these experiments. As large aggregates can block the system, the samples were centrifuged or filtered before the analyses. This changed the sample compositions and removed any large aggregates, which was detected as low sample recoveries. However, even the native samples had sample losses of some percentages. The sample loss was also visible in the chromatograms, as the intensity of the monomer peak decreased, but no additional particles became visible. In addition, the MW range of the column excluded larger aggregates. In terms of separation and MW determination, some dimers were successfully separated from the monomers, and the determined MWs were obtained with low uncertainties. The MWs for the monomer peaks were slightly underestimated and the peaks suffered from tailing in some experiments. With some of the peaks containing larger aggregates, the PDIs indicated that SEC could not separate the contents due to fast equilibrium events occurring in the samples. Some of these peaks

were, on the other hand, homogeneous, but the MWs were not exact multimers of the monomer. This indicates that the monomers in the aggregates had altered in structure. The sample fractions of the aggregates were mainly not in accordance with the probes but either under- or over-estimated. While the hydrodynamic radii obtained with flow mode DLS for most of the monomers were accurate though slightly underestimated, the instrument struggled to obtain them for the other particles. Alternatively, the radii were not compatible with the MWs and had high uncertainties. In addition, in one experiment, SEC-MALS could not produce data for some samples. However, it is likely that some of these problems would have been solved by focusing on method optimization.

The luminescent probes used were sensitive in detecting aggregation in the samples. With the help of standard curves, the signals produced, especially with ProteoStat, could be used to assess the aggregation-% of the samples. Since ProteoStat was designed to be used with the ProteoStat standards, and it also gave similar results to the AT standards, the estimates the probe produced can be considered relatively accurate. In addition, SYPRO Orange gave similar estimates for the aggregation-%s than ProteoStat. The Protein-Probe estimated the aggregation-% of the samples to be lower than SYPRO Orange and ProteoStat. This is likely due to the high specificity of the probe and the small sample volumes used with the method. Since the Protein-Probe interacts with the highest specificity out of the probes, it likely requires a standard curve created from the same mAb used in the aggregation experiments. The S/B-ratios obtained with the FRET-probe varied greatly, with the highest obtained for trastuzumab. Since the Protein-Probe is similar in structure and function to the FRET-probe, it can be deduced that the differences in S/B-ratios between different mAbs will cause a significant undervaluation of the aggregation-%. A 2 µl sample volume used with the Protein-Probe compared to the 98 µl and 28 µl used with ProteoStat and SYPRO Orange, will also cause discrepancies. Homogeneous samples are difficult to obtain with very low sample volumes, and absorption to the pipet is a likely occurrence. Hence, the Protein-Probe likely measured aggregation from a different perspective than the two other probes.

The probe-based protocols were user-friendly and relatively fast to perform. No complex and expensive equipment was needed. Also, the external probes were non-invasive, even though the probes may disturb the aggregate equilibriums. In the case of the ProteoStat and SYPRO Orange, essentially no dilution in the wells occurred due to large sample-to-detection volume ratios. With the Protein-Probe method, a dilution of over 30x occurred in the addition of the detection solution, which may have affected the possible reversible

aggregates depending on the mAb concentrations. The sample consumptions varied significantly, as 49x more sample was required with ProteoStat compared to the Protein-Probe method. Especially the sample consumption of Protein-Probe enables very low material consumption, and a possibility for frequent assay runs with low-concentration samples. The probes do not give direct information about the nature of the aggregates, even though they did display different selectivities.

The different stress conditions used induced various aggregates. The Protein-Probe had a higher sensitivity towards the standards with higher aggregate-% based on the standard curves. This could be related to either the larger size of the aggregates, the presence of more appropriate binding sites, or both. SYPRO Orange showed unusually large S/B-ratios for the low pH aggregates, indicating that the structures differed from those produced by high temperatures. This could mean that the aggregates were amyloid-like, towards which the probe has shown extreme sensitivity[58]. A connection between acidic pH and amyloid formation has been discovered previously[59]. The LLDs obtained from the standard curves suggested the Protein-Probe to be the most sensitive of the probes. The Protein-Probe has been reported to detect < 0.1 % of IgG aggregates[53], which is substantially less than what the ProteoStat manufacturer promises for ProteoStat (1–5%). However, in these experiments, the Protein-Probe seemed to have a similar sensitivity to the other probes with a few exceptions. One explanation for this is the dilution of the sample occurring with the Protein-Probe method. If the samples contained reversible aggregates, it is possible that the dilution caused them to dissociate, and this changed the sample composition. In addition, due to the small sample volume used with Protein-Probe, the samples were likely less homogenous than in larger sample volumes. In conclusion, all the probes seemed to perform equally well in terms of the S/B-ratios, which reflect the sensitivities.

ProteoStat performed the most reliably out of the probes, as the specific mAb structure did not affect the evenly high S/B-ratios it produced. ProteoStat has been reported to be more sensitive towards smaller aggregates[43], which all the experiments seemed to produce. Despite this, the two other probes produced higher S/B-ratios for the aggregates induced by low pH. It could be possible that the probe is not as sensitive toward amyloid-like aggregates. ProteoStat could be used with both standard sets, which is a clear benefit. A downside of the probe is that the sample consumption is relatively high compared to the other probes.

On average, the external probes detected 10x less aggregates present than DLS and SEC-MALS, providing significantly better sensitivity. With the help of aggregation-% standards, they could provide qualitative data with low-cost equipment, simple protocols, and without any separation process. While light scattering-based methods are, in theory, optimal for aggregate studies, either physical or mathematical models for separation are necessary, which both have their downsides. The mathematical models in batch-mode DLS cannot provide sufficient separation in all cases, and physical separation in high-pressure SEC-MALS is not ideal with sensitive samples like aggregates. The information obtained with DLS was qualitative but sometimes very limited depending on the samples. SEC-MALS did not generate much qualitative or quantitative data, as parts of the samples never entered the system. In addition, the separation process was disturbed by the aggregate equilibriums.

The most optimal combination to study aggregation would be DLS with an external probe based on this work. These data combined would give qualitative and quantitative information of aggregation. The concentration working ranges for each particle sizes with DLS should be determined so that the data produced would be as accurate as possible. Considering the dynamic nature of aggregates, any invasive methods should be avoided to obtain results representative of the actual sample composition.

5 References

(1)   Antibody therapeutics approved or in regulatory review in the EU or US - The Antibody Society https://www.antibodysociety.org/resources/approved-antibodies/ (accessed Nov 17, 2021).

(2)   Carrara, S. C.; Ulitzka, M.; Grzeschik, J.; Kornmann, H.; Hock, B.; Kolmar, H. From Cell Line Development to the Formulated Drug Product: The Art of Manufacturing Therapeutic Monoclonal Antibodies. *Int. J. Pharm.* **2021**, *594*, 120164. https://doi.org/10.1016/J.IJPHARM.2020.120164.

(3)   Awwad, S.; Angkawinitwong, U. Overview of Antibody Drug Delivery. *Pharmaceutics* **2018**, *10* (3), 83. https://doi.org/10.3390/PHARMACEUTICS10030083.

(4)   Goswami, S.; Wang, W.; Arakawa, T.; Ohtake, S. Developments and Challenges for MAb-Based Therapeutics. *Antibodies* **2013**, *2* (3), 452–500. https://doi.org/10.3390/ANTIB2030452.

(5)   Shire, S. J. Stability of Monoclonal Antibodies (MAbs). In *Monoclonal Antibodies*; Woodhead Publishing, 2015; pp 45–92. https://doi.org/10.1016/B978-0-08-100296-4.00003-8.

(6)   Roberts, C. J. Therapeutic Protein Aggregation: Mechanisms, Design, and Control. *Trends Biotechnol.* **2014**, *32* (7), 372–380. https://doi.org/10.1016/J.TIBTECH.2014.05.005.

(7)   Creighton, T. E. Protein Folding. *Biochem. J.* **1990**, *270* (1), 1–16. https://doi.org/10.1042/BJ2700001.

(8)   Wang, W.; Roberts, C. J. Protein Aggregation – Mechanisms, Detection, and Control. *Int. J. Pharm.* **2018**, *550* (1–2), 251–268. https://doi.org/10.1016/J.IJPHARM.2018.08.043.

(9)   Philo, J. S. Is Any Measurement Method Optimal for All Aggregate Sizes and Types? *AAPS J.* **2006**, *8* (3), 564–571. https://doi.org/10.1208/AAPSJ080365.

(10)   Raimondi, S.; Guglielmi, F.; Giorgetti, S.; Gaetano, S. Di; Arciello, A.; Monti, D. M.; Relini, A.; Nichino, D.; Doglia, S. M.; Natalello, A.; Pucci, P.; Mangione, P.; Obici, L.; Merlini, G.; Stoppini, M.; Robustelli, P.; Tartaglia, G. G.; Vendruscolo, M.; Dobson, C. M.; Piccoli, R.; Bellotti, V. Effects of the Known Pathogenic Mutations on the Aggregation Pathway of the Amyloidogenic Peptide of Apolipoprotein A-I. *J. Mol. Biol.* **2011**, *407* (3), 465–476. https://doi.org/10.1016/J.JMB.2011.01.044.

(11)   Dekel, Y.; Machluf, Y.; Gefen, T.; Eidelshtein, G.; Kotlyar, A.; Bram, Y.; Shahar, E.; Reslane, F.; Aizenshtein, E.; Pitcovski, J. Formation of Multimeric Antibodies for Self-Delivery of Active Monomers. *Drug Deliv.* **2017**, *24* (1), 199–208. https://doi.org/10.1080/10717544.2016.1242179.

(12)   Cabra, V.; Vázquez-Contreras, E.; Moreno, A.; Arreguin-Espinosa, R. The Effect of Sulfhydryl Groups and Disulphide Linkage in the Thermal Aggregation of Z19 α-Zein. *Biochim. Biophys. Acta - Proteins Proteomics* **2008**, *1784* (7–8), 1028–1036. https://doi.org/10.1016/J.BBAPAP.2008.04.002.

(13)   Esfandiary, R.; Parupudi, A.; Casas-Finet, J.; Gadre, D.; Sathish, H. Mechanism of Reversible Self-Association of a Monoclonal Antibody: Role of Electrostatic and Hydrophobic Interactions. *J. Pharm. Sci.* **2015**, *104* (2), 577–586. https://doi.org/10.1002/JPS.24237.

(14)   Meric, G.; Robinson, A. S.; Roberts, C. J. Driving Forces for Nonnative Protein Aggregation and Approaches to Predict Aggregation-Prone Regions. *Annu. Rev. Chem. Biomol. Eng.* **2017**, *8*, 139–159. https://doi.org/10.1146/ANNUREV-CHEMBIOENG-060816-101404.

(15)   Chaudhuri, R.; Cheng, Y.; Middaugh, C. R.; Volkin, D. B. High-Throughput Biophysical Analysis of Protein Therapeutics to Examine Interrelationships between Aggregate Formation and Conformational Stability. *AAPS J.* **2014**, *16* (1), 48–64. https://doi.org/10.1208/s12248-013-9539-6.

(16)   Blancas-Mejía, L. M.; Misra, P.; Ramirez-Alvarado, M. Differences in Protein Concentration Dependence for Nucleation and Elongation in Light Chain Amyloid Formation. *Biochemistry* **2017**, *56* (5), 757–766. https://doi.org/10.1021/ACS.BIOCHEM.6B01043/SUPPL_FILE/BI6B01043_SI_001.PDF.

(17)   Bee, J. S.; Davis, M.; Freund, E.; Carpenter, J. F.; Randolph, T. W. Aggregation of a Monoclonal Antibody Induced by Adsorption to Stainless Steel. *Biotechnol. Bioeng.* **2010**, *105* (1), 121–129. https://doi.org/10.1002/BIT.22525.

(18)   Sahin, Z.; Demir, Y. K.; Kayser, V. Global Kinetic Analysis of Seeded BSA Aggregation. *Eur. J. Pharm. Sci.* **2016**, *86*, 115–124. https://doi.org/10.1016/J.EJPS.2016.03.007.

(19)   Barnett, G. V.; Qi, W.; Amin, S.; Neil Lewis, E.; Roberts, C. J. Aggregate Structure, Morphology and the Effect of Aggregation Mechanisms on Viscosity at Elevated Protein Concentrations. *Biophys. Chem.* **2015**, *207*, 21–29. https://doi.org/10.1016/J.BPC.2015.07.002.

(20)   Bardin, C.; Astier, A.; Vulto, A.; Sewell, G.; Vigneron, J.; Trittler, R.; Daouphars, M.; Paul, M.; Trojniak, M.; Pinguet, F. Guidelines for the Practical Stability Studies of Anticancer Drugs: A European Consensus Conference. *Eur. J. Hosp. Pharm. Sci. Pract.* **2012**, *19* (3), 278–285. https://doi.org/10.1136/EJHPHARM-2012-000112.

(21)   Philo, J. S. A Critical Review of Methods for Size Characterization of Non-Particulate Protein Aggregates. *Curr. Pharm. Biotechnol.* **2009**, *10*, 359–372. https://doi.org/10.2174/138920109788488815.

(22)   Cheng, W.; Joshi, S. B.; He, F.; Brems, D. N.; He, B.; Kerwin, B. A.; Volkin, D. B.; Middaugh, C. R. Comparison of High-Throughput Biophysical Methods to Identify Stabilizing Excipients for a Model IgG2 Monoclonal Antibody: Conformational Stability and Kinetic Aggregation Measurements. *J. Pharm. Sci.* **2012**, *101* (5), 1701–1720. https://doi.org/10.1002/JPS.23076.

(23)   Brader, M. L.; Estey, T.; Bai, S.; Alston, R. W.; Lucas, K. K.; Lantz, S.; Landsman, P.; Maloney, K. M. Examination of Thermal Unfolding and Aggregation Profiles of a Series of Developable Therapeutic Monoclonal Antibodies. *Mol. Pharm.* **2015**, *12* (4), 1005–1017. https://doi.org/10.1021/MP400666B.

(24)   Duy, C.; Fitter, J. How Aggregation and Conformational Scrambling of Unfolded States Govern Fluorescence Emission Spectra. *Biophys. J.* **2006**, *90* (10), 3704–3711. https://doi.org/10.1529/BIOPHYSJ.105.078980.

(25)   Akazawa-Ogawa, Y.; Nagai, H.; Hagihara, Y. Heat Denaturation of the Antibody, a Multi-Domain Protein. *Biophys. Rev.* **2018**, *10* (2), 255. https://doi.org/10.1007/S12551-017-0361-8.

(26)   Fekete, S.; Beck, A.; Veuthey, J. L.; Guillarme, D. Theory and Practice of Size Exclusion Chromatography for the Analysis of Protein Aggregates. *J. Pharm. Biomed. Anal.* **2014**, *101*, 161–173. https://doi.org/10.1016/J.JPBA.2014.04.011.

(27)   Pothecary, M.; Ball, S.; Clarke, P. Protein Applications for Advanced Multi-Detector Size-Exclusion Chromatography. *Chromatogr. Today* **2012**, No. September, 32–35.

(28)   Larkin, M.; Wyatt, P. . Light-Scattering Techniques and Their Application to Formulation and Aggregation Concerns. In *Formulation and Process Development Strategies for Manufacturing Biopharmaceuticals*; John Wiley & Sons, Inc., 2010; pp 269–305. https://doi.org/10.1002/9780470595886.ch12.

(29)   Aitken, A.; Learmonth, M. Protein Determination by UV Absorption. In *The Protein Protocols Handbook*; Humana Press, 1996; pp 3–6. https://doi.org/10.1007/978-1-60327-259-9_1.

(30)   Some, D. *SEC-MALS for Absolute Biophysical Characterization*.

(31)   SEC-MALS for Absolute Molar Mass and Size Measurements https://www.wyatt.com/solutions/techniques/sec-mals-molar-mass-size-multi-angle-light-scattering.html#sec-mals-2 (accessed May 3, 2022).

(32)   Wyatt, P. J. Light Scattering and the Absolute Characterization of Macromolecules. *Anal. Chim. Acta* **1993**, *272* (1), 1–40. https://doi.org/10.1016/0003-2670(93)80373-S.

(33)   Zhao, H.; Brown, P. H.; Schuck, P. On the Distribution of Protein Refractive Index Increments. *Biophys. J.* **2011**, *100* (9), 2309–2317. https://doi.org/10.1016/J.BPJ.2011.03.004.

(34)   Panchal, J.; Kotarek, J.; Marszal, E.; Topp, E. M. Analyzing Subvisible Particles in Protein Drug Products: A Comparison of Dynamic Light Scattering (DLS) and Resonant Mass Measurement (RMM). *AAPS J.* **2014**, *16* (3), 440–451. https://doi.org/10.1208/S12248-014-9579-6/FIGURES/7.

(35)   Pusey, P. Photon Correlation and Light Beating Spectroscopy. In *Photon Correlation and Light Beating Spectroscopy*; Cummins, H. Z., Pike, E. ., Eds.; Plenum New York, 1972; pp 387–428. https://doi.org/10.1007/978-1-4615-8906-8.

(36)   Stetefeld, J.; McKenna, S. A.; Patel, T. R. Dynamic Light Scattering: A Practical Guide

and Applications in Biomedical Sciences. *Biophys. Rev.* **2016**, *8* (4), 409–427. https://doi.org/10.1007/S12551-016-0218-6/TABLES/3.

(37)   Mahler, H.-C.; Friess, W.; Grauschopf, U.; Kiese, S. Protein Aggregation: Pathways, Induction Factors and Analysis. *J. Pharm. Sci.* **2009**, *98* (9), 2909–2934.

(38)   Arakawa, T.; Ejima, D.; Li, T.; Philo, J. S. The Critical Role of Mobile Phase Composition in Size Exclusion Chromatography of Protein Pharmaceuticals. *J. Pharm. Sci.* **2010**, *99* (4), 1674–1692. https://doi.org/10.1002/JPS.21974.

(39)   Fekete, S.; Ganzler, K.; Guillarme, D. Critical Evaluation of Fast Size Exclusion Chromatographic Separations of Protein Aggregates, Applying Sub-2 Mm Particles. *J. Pharm. Biomed. Anal.* **2013**, *78–79*, 141–149. https://doi.org/10.1016/J.JPBA.2013.02.013.

(40)   Hawe, A.; Sutter, M.; Jiskoot, W. Extrinsic Fluorescent Dyes as Tools for Protein Characterization. *Pharm. Res.* **2008**, *25* (7), 1487–1499. https://doi.org/10.1007/S11095-007-9516-9.

(41)   Le Basle, Y.; Chennell, P.; Tokhadze, N.; Astier, A.; Sautou, V. Physicochemical Stability of Monoclonal Antibodies: A Review. *J. Pharm. Sci.* **2020**, *109* (1), 169–190. https://doi.org/10.1016/J.XPHS.2019.08.009.

(42)   Chi, E. Y.; Krishnan, S.; Randolph, T. W.; Carpenter, J. F. Physical Stability of Proteins in Aqueous Solution: Mechanism and Driving Forces in Nonnative Protein Aggregation. *Pharm Res.* **2003**, *20*, 1325–1336.

(43)   Oshinbolu, S.; Shah, R.; Finka, G.; Molloy, M.; Uden, M.; Bracewell, D. G. Evaluation of Fluorescent Dyes to Measure Protein Aggregation within Mammalian Cell Culture Supernatants. *J. Chem. Technol. Biotechnol.* **2018**, *93* (3), 909–917. https://doi.org/10.1002/JCTB.5519.

(44)   Lakowicz, J. R. *Principles of Fluorescence Spectroscopy*; Springer, 2006. https://doi.org/10.1007/978-0-387-46312-4.

(45)   Das, K.; Sarkar, N.; Nath, D.; Bhattacharyya, K. Non-Radiative Pathways of Anilino-Naphthalene Sulphonates: Twisted Intramolecular Charge Transfer versus Intersystem Crossing. *Spectrochim. Acta Part A Mol. Spectrosc.* **1992**, *48* (11–12), 1701–1705. https://doi.org/10.1016/0584-8539(92)80243-P.

(46)   Selvin, P. R. Principles and Biophysical Applications of Lanthanide-Based Probes. *Annu Rev Biophys Biomol Struct.* **2002**, *31*, 275–302. https://doi.org/10.1146/ANNUREV.BIOPHYS.31.101101.140927.

(47)   Degorce, F.; Card, A.; Soh, S.; Trinquet, E.; Knapik, G. P.; Xie, B. HTRF: A Technology Tailored for Drug Discovery –A Review of Theoretical Aspects and Recent Applications. *Curr. Chem. Genomics* **2009**, *3* (1), 22–32. https://doi.org/10.2174/1875397300903010022.

(48)   Gudgin Dickson, E. F.; Pollak, A.; Diamandis, E. P. Time-Resolved Detection of Lanthanide Luminescence for Ultrasensitive Bioanalytical Assays. *J. Photochem. Photobiol. B Biol.* **1995**, *27* (1), 3–19. https://doi.org/10.1016/1011-1344(94)07086-4.

(49)   Stryer, L. The Interaction of a Naphthalene Dye with Apomyoglobin and Apohemoglobin: A Fluorescent Probe of Non-Polar Binding Sites. *J. Mol. Biol.* **1965**, *13* (2), 482–495. https://doi.org/10.1016/S0022-2836(65)80111-5.

(50)   Matulis, D.; Lovrien, R. 1-Anilino-8-Naphthalene Sulfonate Anion-Protein Binding Depends Primarily on Ion Pair Formation. *Biophys. J.* **1998**, *74* (1), 422–429. https://doi.org/10.1016/S0006-3495(98)77799-9.

(51)   Mora, A. K.; Nath, S. Understanding the Amyloid Sensing Mechanism of SYPRO Orange.

Dye. Pigment. **2021**, *194*, 109585. https://doi.org/10.1016/J.DYEPIG.2021.109585.

(52) Enzo Life Sciences, I. *W ENZ-51023 Quantitative Detection of Protein Aggregates from Visible to Subvisible Particles*.

(53) Valtonen, S.; Vuorinen, E.; Eskonen, V.; Malakoutikhah, M.; Kopra, K.; Härmä, H. Sensitive, Homogeneous, and Label-Free Protein-Probe Assay for Antibody Aggregation and Thermal Stability Studies. *MAbs* **2021**, *13* (1), 1955810. https://doi.org/10.1080/19420862.2021.1955810.

(54) Joshi, S.; Maharana, C.; Rathore, A. S. An Application of Nano Differential Scanning Fluorimetry for Higher Order Structure Assessment between MAb Originator and Biosimilars: Trastuzumab and Rituximab as Case Studies. *J. Pharm. Biomed. Anal.* **2020**, *186*, 113270. https://doi.org/10.1016/J.JPBA.2020.113270.

(55) Armstrong, J. K.; Wenby, R. B.; Meiselman, H. J.; Fisher, T. C. The Hydrodynamic Radii of Macromolecules and Their Effect on Red Blood Cell Aggregation. *Biophys. J.* **2004**, *87* (6), 4259. https://doi.org/10.1529/BIOPHYSJ.104.047746.

(56) Ahmadi, M.; Bryson, C. J.; Cloake, E. A.; Welch, K.; Filipe, V.; Romeijn, S.; Hawe, A.; Jiskoot, W.; Baker, M. P.; Fogg, M. H. Small Amounts of Sub-Visible Aggregates Enhance the Immunogenic Potential of Monoclonal Antibody Therapeutics. *Pharm. Res.* **2015**, *32* (4), 1383–1394. https://doi.org/10.1007/S11095-014-1541-X.

(57) Brorson, K.; Krejci, S.; Lee, K.; Hamilton, E.; Stein, K.; Xu, Y. Bracketed Generic Inactivation of Rodent Retroviruses by Low PH Treatment for Monoclonal Antibodies and Recombinant Proteins. *Biotechnol. Bioeng.* **2003**, *82* (3), 321–329. https://doi.org/10.1002/BIT.10574.

(58) Mora, A. K.; Nath, S. SYPRO Orange-a New Gold Standard Amyloid Probe. *J. Mater. Chem. B* **2020**, *8* (35), 7894–7898. https://doi.org/10.1039/D0TB01406K.

(59) Su, Y.; Chang, P. T. Acidic PH Promotes the Formation of Toxic Fibrils from β-Amyloid Peptide. *Brain Res.* **2001**, *893* (1–2), 287–291. https://doi.org/10.1016/S0006-8993(00)03322-9.